Geoscience Frontiers 11 (2020) 925–942

Contents lists available at ScienceDirect

Geoscience Frontiers

journal homepage: www.elsevier.com/locate/gsf

Research Paper

Lead isotope evolution of the Central European upper mantle: Constraints from the Bohemian Massif

Simona Krmíčková [a,b], Lukáš Krmíček [a,b,c,*], Rolf L. Romer [d], Jaromír Ulrych [b]

[a] Department of Geological Sciences, Faculty of Science, Masaryk University, Kotlářská 2, CZ-611 37, Brno, Czech Republic
[b] Institute of Geology of the Czech Academy of Sciences, Rozvojová 269, CZ-165 02, Prague 6, Czech Republic
[c] Brno University of Technology, Faculty of Civil Engineering, AdMaS Centre, Veveří 95, CZ-602 00, Brno, Czech Republic
[d] Deutsches GeoForschungsZentrum GFZ, Telegrafenberg, D-144 73, Potsdam, Germany

ARTICLE INFO

Handling Editor: Christopher J Spencer

Keywords:
Lead isotopes
Lamprophyres
Volcanic rocks
Mantle components
Bohemian massif
Variscan orogeny

ABSTRACT

The Pb isotope composition of the upper mantle beneath Central Europe is heterogeneous due to the subduction of regionally contrasting material during the Variscan and Alpine orogenies. Late Variscan to Cenozoic mantle-derived melts allow mapping this heterogeneity on a regional scale for the last ca. 340 Myr. Late Cretaceous and Cenozoic anorogenic magmatic rocks of the Bohemian Massif (lamprophyres, volcanic rocks of basanite/tephrite and trachyte/phonolite series) concentrate mostly in the Eger Rift. Cretaceous ultramafic lamprophyres yielded the most radiogenic Pb isotope signatures reflecting a maximum contribution from metasomatised lithospheric mantle, whereas Tertiary alkaline lamprophyres originated from mantle with less radiogenic $^{206}Pb/^{204}Pb$ ratios suggesting a more substantial modification of lithospheric source by interaction with asthenospheric-derived melts. Cenozoic volcanic rocks of the basanite/tephrite and trachyte/phonolite series define a linear mixing trend between these components, indicating dilution of the initial lithospheric mantle signature by upwelling asthenosphere during rifting. The Pb isotope composition of Late Cretaceous and Cenozoic magmatic rocks of the Bohemian Massif follows the same Pb growth curve as Variscan orogenic lamprophyres and lamproites that formed during the collision between Laurussia, Gondwana, and associated terranes. This implies that the crustal Pb signature in the post-Variscan mantle is repeatedly sampled by younger anorogenic melts. Most Cenozoic mantle-derived rocks of Central Europe show similar Pb isotope ranges as the Bohemian Massif.

1. Introduction

Central Europe has been affected by two major extensional events of Permo-Carboniferous and Tertiary age (e.g., Meier et al., 2016). Permo-Carboniferous extension began in Central Europe because of post-collisional changes in the kinematics between the Laurussia and the Gondwana plates (Kroner et al., 2016) and resulted in the formation of the Central European Extensional Province (CEEP) with numerous volcano-sedimentary basins in Europe as well as the Oslo Rift (e.g., Neumann et al., 2004; Wilson et al., 2004). This extension was coeval with the opening of the Palaeo-Tethys Ocean farther to the east and the closure of the remaining Rheic Ocean farther to the west (Kroner and Romer, 2013). Late Cretaceous to Tertiary lithospheric extension was initiated as a response to the tensional reactivation of Variscan Permo-Carboniferous fracture systems by the Alpine collision, eventually resulting in the formation of a vast rift system in Western and Central Europe. The European Cenozoic rift system includes the following individual rifts: Valencia Trough in Spain, the Gulf of Lions, the Saône, Limagne and Bresse grabens in south-eastern France, the Rhine, Ruhr and Leine grabens in Germany, and the Eger Rift in the Bohemian Massif (Ziegler, 1992, Fig. 1).

Formation of continental rift systems associated with horizontal movements of plates and subsequent lithosphere thinning is commonly accompanied with magma generation by decompression melting of lithospheric and asthenospheric mantle that is passively upwelling beneath the thinned lithosphere (e.g., Berkesi et al., 2019). Melts generated in rifts by decompression are separated from their residue and ascend from the zone of melting in the upper mantle and are emplaced within the overlying continental crust or are extruded as lava flows. The volume of the produced melts depends on the amount of lithospheric

* Corresponding author. Institute of Geology of the Czech Academy of Sciences, Rozvojová 269, CZ-165 02, Prague 6, Czech Republic.
E-mail address: lukas.krmicek@gmail.com (L. Krmíček).
Peer-review under responsibility of China University of Geosciences (Beijing).

https://doi.org/10.1016/j.gsf.2019.09.009
Received 27 April 2019; Received in revised form 2 August 2019; Accepted 25 September 2019
Available online 23 October 2019

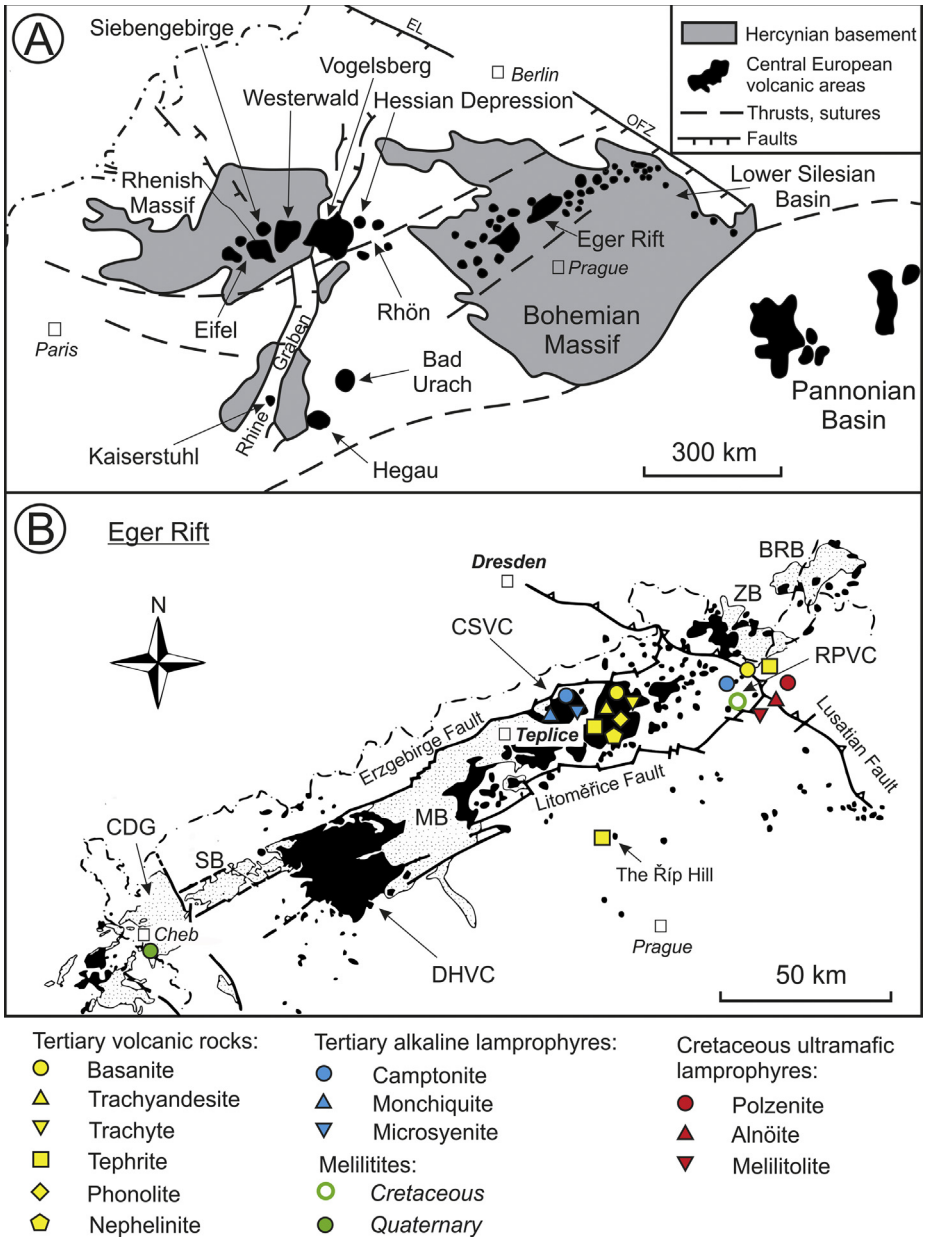

Fig. 1. (A) Distribution of major volcanic areas within Central Europe (modified after Blusztajn and Hegner, 2002); EL – Elbe Line, OFZ – Odra Fault Zone. (B) Map of volcanic centres in the Eger Rift with sampling areas (modified after Zachariáš et al., 2008). Abbreviations: BRB – Berzdorf Radomierzyce Basin; CDG – Cheb–Domažlice Graben; CSVC – České Středohoří Volcanic Complex; DHVC – Doupovské Hory Volcanic Complex; MB – Most Basin; RPVC – Ralská Pahorkatina Volcanic Complex; SB – Sokolov Basin; ZB – Zittau Basin.

extension and on the temperature of the asthenosphere. The primary products of volcanic activity in rifts are mainly basaltic. Continental intra-plate rifting produces predominantly olivine/nepheline-bearing alkaline basalts (e.g., White and McKenzie, 1989; Wilson and Downes, 1992; Lustrino and Wilson, 2007; Haase and Renno, 2008).

For the Cenozoic rift system of the Central European Volcanic Province (CEVP), there are two end-member type models. Some authors favour asthenospheric melting in response to large-scale upwelling of mantle plumes or small-scale plumelets (e.g., Wilson and Downes, 1991; Hegner et al., 1995). Other studies favour derivation of the intraplate volcanic rocks from the metasomatised lithospheric mantle, either by preferential melting of phlogopite/amphibole-bearing vein assemblages hosted in lherzolitic mantle or by very low degree melting of highly metasomatised domains, resulting in the generation of strongly SiO_2-undersaturated melts (Hegner et al., 1995; Jung et al., 2005; Pfänder et al., 2018).

Late Variscan to Cenozoic mantle-derived rocks, such as lamprophyres, lamproites, and alkali-basalts, largely sampled the same mantle on a regional scale and at variable depth during above mentioned extensional events (e.g., Mayer et al., 2014; Krmíček et al., 2016; Ulrych et al., 2018). Although mantle-derived lamprophyres and associated intrusive rocks are relatively rare within the volcanic complexes, these small-volume melts are particularly important for studying processes and geochemical heterogeneities of the upper mantle beneath Central Europe as they preferentially sample the metasomatic component, which was induced during the Variscan orogeny when continental collision brought continental crust to mantle depth (e.g., Kroner and Romer, 2013; Borghini et al., 2018; Pfänder et al., 2018).

The Sr, Nd, and Pb isotope composition of mantle-derived rocks may identify contributions from different mantle sources, such as depleted asthenospheric and enriched lithospheric upper mantle and lower mantle, to the generated magmas (e.g., White and McKenzie, 1989; Zou et al., 2000). Isotope constraints on the mantle sources of Mesozoic and Cenozoic volcanic rocks of the Bohemian Massif largely rely on Sr–Nd isotope data (e.g., Alibert et al., 1983, 1987; Blusztajn and Hart, 1989; Bendl et al., 1993; Vokurka, 1997; Ulrych et al., 2002, 2008, 2011, 2013, 2016, 2018; Haase and Renno, 2008; Cajz et al., 2009; Skála et al., 2014, 2015). In contrast, Pb isotope data are rare (Blusztajn and Hart, 1989;

Haase and Renno, 2008; Ulrych et al., 2016). As typical mantle has low Pb contents, the Pb isotope composition of the mantle is readily affected during metasomatism. Because of the contrasting Pb contents in crust and mantle rocks, small contributions of continental material are more sensitively recorded in the Pb isotope composition than in the Sr and Nd isotope composition (Cohen and O'Nions, 1982; Davies and Macdonald, 1987; Sun and McDonough, 1989; Conticelli et al., 2002).

Our paper focuses on Pb isotope data and whole-rock geochemistry of intrusive and extrusive volcanic rocks of the Bohemian Massif that sampled the upper mantle. We pay special attention whether Late Palaeozoic to Quaternary Central European mantle-derived rocks sampled different mantle sources on a local to regional scale and through time.

2. Geological setting

The upper mantle beneath Central Europe is heterogeneous, which is largely due to Variscan and Alpine subduction events during which regionally contrasting subducted material of both continental and oceanic crust metasomatically modified the upper mantle (e.g., Wit-t-Eickschen and Kramm, 1997; Downes, 2001; Ackerman et al., 2009; Kroner and Romer, 2013; Pfänder et al., 2018). Older tectonic structures reactivated during the late Variscan to Alpine events were associated with asthenospheric upwelling and subsequent extension-related magmatism that sampled this modified mantle (Wilson and Downes, 1991).

2.1. Variscan to post-Variscan development

The Variscan orogen is the result of the Devonian–Carboniferous collision of Gondwana with Laurussia that started with the collision of the Armorican Spur, which is part of segmented peri-Gondwana. The collision of the Armorican Spur with Laurussia resulted in the closure of the Rheic Ocean in the area of future Central Europe (Kroner and Romer, 2010, 2013). The subducted material consisted primarily of relative thin lithosphere covered by Palaeozoic volcano-sedimentary rocks (Kroner et al., 2007). In contrast, the unsubductable parts of the peri-Gondwana (Cadomian) magmatic arc (i.e., thick crustal fragments of the Armorican Spur) caused reorganisation within the plate boundary zone (Kroner and Romer, 2013). The Bohemian Massif consists of high- and low-strain domains that behaved differently during the Variscan orogeny. The Teplá-Barrandian Unit and Lusatia (parts of Gondwana) and the Brunovistulian Terrane (part of Laurussia) are low-strain domains that collided during the closure of the Rheic ocean (e.g., Kalvoda et al., 2008; Kalvoda and Bábek, 2010). The Saxo-Thuringian and Moldanubian Zones are high-strain domains that represent former Gondwana shelf and that were subducted and exhumed during the Variscan orogeny (e.g., Kroner and Romer, 2013; Krmíček et al., 2016; Žák and Sláma, 2018).

Plate tectonic processes that may have changed the composition of the upper mantle of the Bohemian Massif include (i) Cadomian subduction followed by Late Neoproterozoic back-arc spreading and early Palaeozoic rifting in northern peri-Gondwana, (ii) intra-oceanic subduction and formation of oceanic arcs that were later accreted to form part of Variscan Europe, (iii) possible subduction beneath the northwards migrating terranes, (iv) subduction and collision at the southern margin of Laurussia, and (v) Carboniferous extension of Central Europe (Wilson et al., 2004; McCann et al., 2006; Pin and Waldhausrová, 2007; Timmerman, 2008; Abdelfadil et al., 2013; Dostal et al., 2019a,b). Subduction of both oceanic and continental crust peaked at 340 Ma and led to the establishment of isotopically contrasting domains in the metasomatised lithospheric mantle (Krmíček et al., 2016). During the late stage of the Variscan orogeny, these metasomatised mantle domains underwent partial melting resulting at ca. 340–300 Ma in the intrusion of potassic to ultrapotassic dykes (lamprophyres and lamproites) along deep-fault zones related to initial crustal extension eventually leading to the formation of the CEEP (Awdankiewicz, 2007, 2009; Krmíček et al., 2011, 2014, 2016; Abdelfadil et al., 2013; Hrouda et al., 2016).

Post-Variscan magmatic activity throughout Variscan Europe was associated with the extension of thickened Variscan crust and accompanied by progressively increasing contributions from the asthenospheric mantle (Lorenz and Nicholls, 1984; Timmerman et al., 2009). Permian extension led to the formation of rift basins, such as the North Germany Basin or the Oslo Rift (Benek et al., 1996; McCann et al., 2006).

2.2. Mesozoic to Cenozoic development

Within the framework of the African–Eurasian plate collision, the extensive European Cenozoic Rift System (ECRIS) formed in Western and Central Europe stretching from Spain and France through Germany to the Czech Republic and Poland (Prodehl et al., 2006). The ECRIS recorded intermittent sub-volcanic/volcanic activities that started in the Late Cretaceous and have lasted to the present (Lustrino and Wilson, 2007). Episodic volcanism occurred mainly in the Oligocene to Miocene with waning phases of anorogenic volcanic activity reaching to the Plio-Pleistocene (Nowell et al., 2006). Magmatic activity in the ECRIS is concentrated in intrusive complexes and volcanic fields within the grabens and their shoulders (Fig. 1A). Rifts formed at reactivated Variscan suture zones separating large different lithospheric segments, indicating structural control on the location of Cenozoic volcanic activity (Dèzes et al., 2004).

The Bohemian Massif is transected by the nearly 300 km long ENE–WSW trending Eger Rift, by the transverse NW–SE striking Elbe/Labe–Odra Fault System in the north (Fig. 1A), and by the NW–SE trending Cheb–Domažlice Graben in the west (Špaček et al., 2011). The Eger Rift represents the easternmost part of the Cenozoic rift system of the Central European Volcanic Province (e.g., Ziegler, 1994; Lustrino and Wilson, 2007). The magmatic rocks of the Eger Rift are predominantly SiO_2-undersaturated alkaline rocks of intra-plate origin (Ulrych et al., 2002, 2011; Lustrino and Wilson, 2007; Dostal et al., 2017). The volcanic activity is a result of reactivation of Variscan structures in the Bohemian Massif during the Alpine orogeny (Babuška and Plomerová, 1992, 2001, 2010). Whether the model of mantle plumes *sensu* Wilson and Paterson (2001), with Alpine flexure and lithospheric extension followed by adiabatic decompression, decompression melting, and injection of mantle-derived magmas into the crust, played a major role is debated (Wilson and Downes, 1991; Wedepohl et al., 1994; Lustrino and Wilson, 2007; Ulrych et al., 2011) and is reflected in terms like Common Mantle Reservoir (CMR – Lustrino and Wilson, 2007) or European Asthenospheric Reservoir (EAR – Cebrià and Wilson, 1995) used to characterise magmas from a possible sub-lithospheric source region.

Ulrych and Pivec (1997) and Ulrych et al. (2011) defined three phases of Cenozoic volcanic activity based on K–Ar dating and palaeostress mapping: (i) a pre-rift period (~80–49 Ma), (ii) a syn-rift period (42–16 Ma) and (iii) a late-rift period (16–0.26 Ma). Ulrych and Pivec (1997) also defined two coeval alkaline series: (i) a volumetrically dominant nephelinite–basanite–tephrite–phonolite series of strongly to mildly alkaline rocks and (ii) a subordinate and only locally occurring weakly alkaline alkali basalt–trachybasalt–trachyandesite–trachyte–rhyolite series. The Eger Rift comprises several volcanic centres (Fig. 1B), namely the České Středohoří Volcanic Complex (CSVC), the Doupovské Hory Volcanic Complex (DHVC; access to volcanic edifice exposures is restricted as they are predominately located in the Doupovské Hory military training zone), the Ralská Pahorkatina Volcanic Complex (RPVC) and a great number of isolated volcanoes in the western part of the Bohemian Cretaceous Basin and in the Cheb–Domažlice Graben (CDG). The youngest volcanoes occur in the Cheb/Eger Basin, a sub-basin of the Eger Rift.

The first manifestation of volcanic activity in the Eger Rift is Late Cretaceous ultramafic lamprophyres and related melilitic rocks associated with subsurface intrusion of melilitolite composition that occur near the intersection of the marginal fault of the Eger Rift and the Lusatian Fault within the future RPVC in the northern part of the Bohemian Cretaceous Basin (Ulrych et al., 2014). Most of the Cenozoic volcanic rocks, predominantly of basanitic composition, are concentrated in the

CSVC and DHVC, whereas hypabyssal intrusions spatially associated with alkaline lamprophyre dykes of Cenozoic age are restricted to the CSVC and RPVC (Skála et al., 2014). Sr-Nd-(Pb)-isotope compositions of rocks from the western Eger Rift, i.e., the DHVC and CDG, were recently published by Ulrych et al. (2016) and Haase et al. (2017). For locations of investigated samples and characteristics of sampled areas see Fig. 1B and Supplement A.

3. Methods

Representative samples of the studied volcanic and subvolcanic rocks are described petrographically using conventional optical microscopy and characterised geochemically by whole-rock and mineral composition using ICP-ES, ICP-MS, and electron microprobe, respectively.

Whole-rock chemical analyses from fresh samples lacking signs of alteration or wall-rock assimilation were carried out at Bureau Veritas (former ACME) Analytical Laboratories Ltd. (Vancouver, Canada) using inductively coupled plasma emission spectrometry (ICP-ES; major oxides, Ba, Ni, Cu, Pb, Zn) and inductively coupled plasma mass spectrometry (ICP-MS; Co, Cs, Hf, Nb, Rb, Sr, Ta, Th, U, V, Zr, Y and REE). Loss on ignition (LOI) was determined by weight difference after ignition at 1000 °C. The Pb, U, and Th concentrations are used to recalculate the initial Pb isotope composition. The errors for the Pb, U and Th concentrations correspond to ±0.1 ppm, ± 0.1 ppm, and ±0.2 ppm, respectively. For further analytical details and detection limits see www.acmelab.com.

The composition of characteristic dark minerals (amphibole, clinopyroxene, and mica) was analysed using a CAMECA SX 100 electron microprobe (Institute of Geology of the CAS, Prague) operated in wavelength-dispersive mode. Measurements were performed using a 15 keV acceleration voltage, 10 nA beam current and 2 μm beam diameter. Both natural and synthetic minerals were used as reference standards. Concentrations of following elements were measured (standard, spectrometer crystals and detection limit for analysed elements are given in parentheses): Si (diopside, LTAP, 222 ppm), Ti (rutile, LPET, 357 ppm), Al (jadeite, LTAP, 272 ppm), Cr (Mn–Cr spinel, LIF, 910 ppm), Fe (haematite, LIF, 1047 ppm), Mn (rhodonite, LIF, 965 ppm), Ni (Ni_2Si, LTAP, 1404 ppm), Mg (periclase, LTAP, 422 ppm), Ca (diopside, LPET, 341 ppm), Na (jadeite, LTAP, 262 ppm), K (leucite, LPET, 300 ppm), F (fluorite, PC0, 1575 ppm), Cl (tugtupite, LPET, 320 ppm), Rb (RbCl, LTAP, 217 ppm) and Ba (barite, LPET, 503 ppm). Counting times on peaks were 10 s for Mg, Al, K, Ca, Cl, Ti; 20 s for Na, Si, Rb, Ba, Ni and Mn, Ni; and 30 s for Cr, Ca and Al. The X-phi correction procedure (Merlet, 1992) was used for spectra processing.

The Pb isotope compositions were determined at Deutsches GeoForschungsZentrum (GFZ), Potsdam, Germany. Powders from representative unaltered samples of volcanic and subvolcanic rocks were dissolved in concentrated HF for four days on a hot plate at 160 °C. Samples were dried, re-dissolved in 2 N HNO_3 and dried slowly at 80 °C overnight to convert fluorides to nitrates. Finally, the samples were taken up in 6 N HCl to convert nitrates to chlorides. Lead was separated in columns using ion exchange resin Bio Rad AG-1-X8. Procedures for the separation and purification of Pb are described in detail by Romer et al. (2005). The ion exchange procedure was repeated to purify Pb elutes. Lead was loaded together with H_3PO_4 and silica-gel emitter on single Re-filaments. The Pb isotope ratios were measured using a Thermo-Finnigan Scientific TRITON TIMS multi-collector mass-spectrometer operated in static multi-collection mode. The obtained Pb isotope ratios were corrected for instrumental fractionation of 0.1%/a.m.u. as determined from repeated measurement of Pb reference material NBS 981. Total procedural blank is between 15 and 30 pg Pb, thus, negligible. Accuracy of the determined Pb data is better than 0.1% at the 2σ level.

4. Results

4.1. Field and petrographic descriptions

The studied volcanic rocks were mainly taken from exposures and quarries (Fig. 2A and B), whereas lamprophyres and related dykes were mostly collected as loose angular blocks in the field (Fig. 2C). Melilitolite sample (OC-12) originates from a 271 m deep Holičský vrch borehole near Osečná (Table 1).

Late Cretaceous ultramafic lamprophyres, such as polzenite and alnöite dykes and the melilitolite of the Osečná intrusion, were sampled in the RPVC. Polzenites and alnöites generally have a fine-grained greyish groundmass and microporphyritic textures. They contain abundant partially serpentinised olivine phenocrysts/xenocrysts in a fine-grained poikilitic groundmass containing microphenocrysts of phlogopite, which may be variably chloritised, flow-oriented melilite laths, feldspathoids, apatite and abundant Ti-rich magnetite (Fig. 2D). Alnöites contain, in contrast to polzenites, also phenocrysts of clinopyroxene.

Tertiary basaltic volcanic rocks predominantly have microporphyritic textures with a fine-grained groundmass. Basanite samples are generally dominated by clusters of slightly serpentinised olivine along with elongated brownish, rarely corroded clinopyroxene crystals with oscillatory and/or hour-glass zoning. Twinned clinopyroxene forms isolated crystals or larger glomerophyres. The basanite fine-grained groundmass contains tiny plagioclase laths irregularly distributed together with smaller clinopyroxene columns (Fig. 2E). Most of the tephrite samples are characterised by the presence of both euhedral and partially corroded kaersutite with apatite inclusions. Kaersutite is surrounded by a very fine-grained hypocrystalline groundmass.

Tertiary alkaline lamprophyres, such as camptonite, monchiquite and more alkaline leucocratic microsyenite, are especially common in the Roztoky Intrusive Complex of the CSVC. A special form of camptonite to monchiquite dykes occurs in the RPVC. The alkaline lamprophyres typically contain macroscopic amphibole phenocrysts in a fine-grained groundmass. The amphibole phenocrysts typically show corrosion rims comprising Ti-rich magnetite. Clinopyroxene in camptonites forms oscillatory and hour-glass zoned phenocrysts and smaller tabular crystals in a fine-grained plagioclase-rich groundmass. A typical accessory mineral is apatite, which is commonly associated with amphibole and/or clinopyroxene, titanomagnetite and feldspathoids. Zeolites are rare and form vesicular fillings (Fig. 2F). Camptonite to monchiquite samples from RPVC are characterised by amphibole that is rimmed by distinct dark mica, strongly serpentinised olivine and rare oscillatory-zoned clinopyroxene in a glassy matrix. Leucocratic microsyenite samples contain glomerophyres of amphibole and alkaline feldspar in a fine-grained feldspar-rich matrix (Fig. 2G). Amphiboles have inclusions of apatite and ilmenite. The groundmass consists primarily of glass, plagioclase and rare sodalite. Vesicles are filled by hydrothermal calcite. Very fine-grained chilled margins of the leucocratic microsyenite dyke show flow-aligned alkali feldspar microphenocrysts (Fig. 2A).

Additionally, two areas with nephelinte to melilitite occurrences are included in this study. Cretaceous intrusive melilitite from the Great Devil's Wall in the RPVC is spatially related to ultramafic lamprophyres and forms a spectacular wall with horizontal columnar jointing (Fig. 2H). It contains mildly corroded olivine often forming clusters, and strongly zoned brown Ti-rich clinopyroxene commonly displaying characteristic twinning. Opaque minerals and flow-oriented thin laths of clinopyroxene occur in a melilite-bearing groundmass. In contrast, the Quaternary melilitite effusion from the youngest volcanic field in the Bohemian Massif, i.e., Cheb Basin, is characterised by the mineral association olivine (with thick, corroded rims) and large, kink-banded phlogopite flakes distributed in a vesicular glassy groundmass. For detailed petrographical characteristic of individual studied samples see Supplement B.

4.2. Mineral chemistry of amphibole, clinopyroxene and dark mica

Chemical compositions of amphibole, clinopyroxene and dark mica from camptonite/monchiquite, leucocratic microsyenite and polzenite samples are listed in Supplement C available in the electronic appendix. Analysed minerals have relatively homogenous compositions without significant variation between cores and rims.

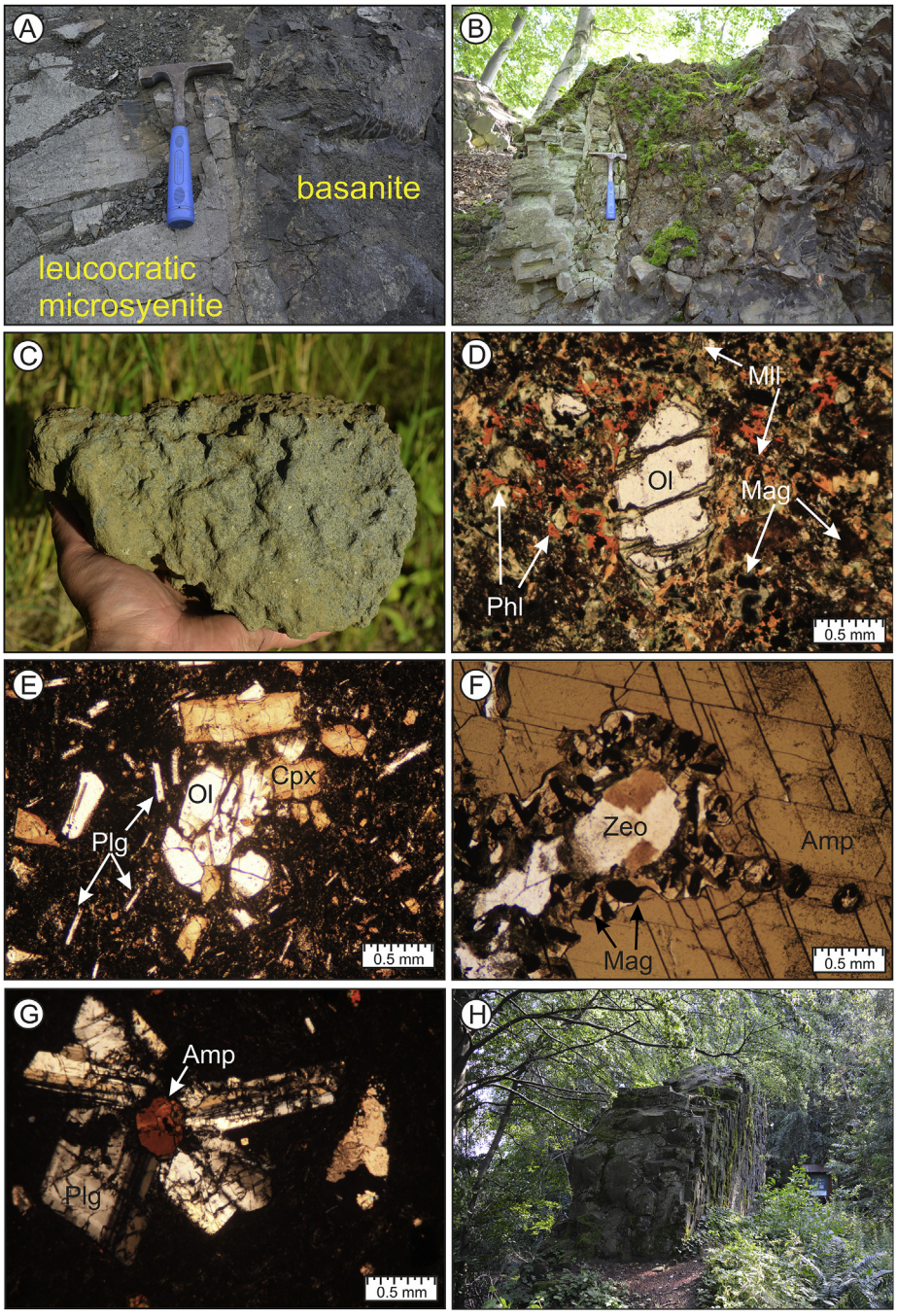

Fig. 2. Field appearances and petrographic features of intrusive (lamprophyric) and extrusive volcanic rocks from the České Středohoří (CSVC) and Ralská Pahorkatina (RPVC) volcanic complexes. (A) Contact of a leucocratic microsyenite dyke in basanite host, characterised by a very fine-grained chilled margin (CSVC). (B) Columnar jointing of sandstone (see Velázquez et al., 2008) at the contact to a camptonite dyke (RPVC). (C) Polzenite with characteristic warty surface (RPVC). (D) Partly serpentinised olivine (Ol) within fine-grained groundmass with slightly chloritised phlogopite (Phl), melilite (Mll) and Ti-rich magnetite (Mag) in polzenite (PPL; RPVC). (E) Cluster of olivine (Ol) and clinopyroxene (Cpx) displaying hour-glass zoning in groundmass composed of smaller plagioclase (Plg) laths and tiny clinopyroxene in basanite (PPL; RPVC). (F) Large amphibole (Amp) phenocryst surrounded by corrosion rim with Ti-rich magnetite (Mag) which encloses rounded vesicles filled with zeolite (Zeo) in camptonite (PPL; RPVC). (G) Glomeroporphyritic amphibole (Amp) and plagioclase (Plg) in aphanitic groundmass in leucocratic microsyenite (XPL; CSVC). (H) The Great Devil's Wall melilitite dyke displaying horizontal columnar jointing (RPVC).

Amphibole phenocrysts from both camptonite/monchiquite and leucocratic microsyenite samples have relatively uniform contents of CaO (11.6–12.8 wt.%) and Na_2O (1.9–2.5 wt.%). Amphibole from leucocratic microsyenite has higher concentrations of FeO^{tot} (13.6–15.3 wt.%) and TiO_2 (4.6–5 wt.%) and lower contents of MgO (10–11.2 wt.%) and Al_2O_3 (12–13.4 wt.%) than those from camptonite/monchiquite samples that have concentrations of MgO = 13–15.2 wt.%, Al_2O_3 = 13.6–14.6 wt.% and TiO_2 = 3.6–4.1 wt.%, except for three analyses that yielded very high TiO_2 contents of 6–6.5 wt.%. Concentrations of FeO^{tot} in amphibole from camptonite/monchiquite samples are between 7.4 wt.% and 10.4 wt.%. All analysed amphibole crystals have high Mg/(Mg + Fe) atomic ratios between 0.54 and 0.82 and have ~6 Si atoms per formula unit (apfu) and ~2 Ca apfu, respectively (Supplement C.1). Analysed amphiboles correspond both to pargasite and kaersutite (Fig. 3A).

Clinopyroxene phenocrysts from camptonite/monchiquite and leucocratic microsyenite samples have similar compositions (Supplement C.2). They are Ca-rich with a relatively narrow range of CaO contents (22.4–24.8 wt.%; ~1 Ca apfu) along with variable concentrations of MgO (7.8–14.2 wt.%), Al_2O_3 (4.8–13.1 wt.%), FeO^{tot} (5.6–10.4 wt.%) and TiO_2 (1.4–5.1 wt.%). They have only minor MnO (up to 0.4 wt.%) and Na_2O (below 1 wt.%) contents. Their Fe/(Fe + Mg) atomic ratios range between 0.19 and 0.43. All analysed clinopyroxene phenocrysts fall in the diopside field (Fig. 3B).

Dark mica from the polzenite sample shows a broad variation in MgO (16.8–22.2 wt.%; ~1.8–2.4 Mg apfu) and Al_2O_3 (11–16.3 wt.%), and plots in two compositional fields (see Fig. 3C). In contrast, dark mica from camptonite/monchiquite is relatively uniform, having MgO and Al_2O_3 contents in the ranges of 16.3–17.3 wt.% and 15.9–16.4 wt.%, respectively. The K_2O contents are more variable in mica from polzenite

Table 1
List of mantle-derived rocks of the Bohemian Massif selected for Pb isotope determination, sample location, petrographic types and field characteristics.

No.	Sample	Locality	Area	Rock type	Age (Ma)	Latitude (N)	Longitude (E)	Outcrop characteristic
1	1_1367	Všechlapy	CSVC	basanite	41.9	50°37.100′	13°47.767′	Quarry
2	4_New	Radobýl	CSVC	basanite	30	50°31.850′	14°05.717′	Abandoned quarry
3	5_New	Soutěsky	CSVC	basanite	30	50°44.883′	14°16.017′	Quarry
4	8_1299	Žandov	CSVC	basanite	25.4	50°42.483′	14°23.817′	Quarry
5	12_1295	Radešín	CSVC	trachybasalt	26.8	50°41.883′	14°03.567′	Abandoned quarry
6	14_1358	Valkeřice	CSVC	trachybasalt	24.7	50°42.117′	14°19.717′	Rock exposure
7	15_1359	Chlum	CSVC	tephrite	26.6	50°44.817′	14°13.583′	Abandoned quarry
8	17_BM-8	Rýdeč	CSVC	phonolite	25.8	50°36.433′	14°09.300′	Abandoned quarry
9	18_BM-16	Štrbický vrch	CSVC	phonolite	30	50°33.467′	13°50.517′	Rock exposure
10	19_BM-48	Bořeň	CSVC	phonolite	30	50°31.617′	13°45.717′	Rock exposure
11	20_BM-13	Lhenice	CSVC	trachyte	30	50°34.500′	13°52.183′	Rock exposure
12	21_BM-51	Milešovský Kloc	CSVC	trachyte	30	50°32.350′	13°55.067′	Rock exposure
13	23_BM-4	Kalich	CSVC	trachyandesite	31	50°36.183′	14°12.567′	Abandoned quarry
14	25_BM-60	Boreč	CSVC	trachyandesite	30	50°30.850′	13°59.267′	Rock exposure
15	CS-30	Dobkovice I	CSVC	monchiquite	30	50°42.633′	14°11.567′	Dyke in old quarry
16	CS-31	Dobkovice II	CSVC	camptonite	30	50°42.640′	14°11.549′	Dyke in old quarry
17	CS-43	Leština	CSVC	camptonite	30	50°39.367′	14°12.300′	Abandoned quarry
18	KK1	Komorní Hůrka	CHB	melilitite	1	50°06.020′	12°20.166′	Rock exposure
19	KK2	Říp	CSVC	tephrite	25.6	50°23.230′	14°17.320′	Angular blocks
20	KK3	Panská skála	CSVC	basanite	29.7	50°46.146′	14°29.102′	Abandoned quarry
21	KK4	Tlustec	RPVC	basanite	30	50°43.535′	14°44.649′	Angular blocks
22	KK5	Stříbrník	RPVC	tephrite	30	50°43.936′	14°50.925′	Rock exposure
23	KK6	Janův Důl	RPVC	camptonite/monchiquite	28.7	50°42.102′	14°57.379′	Abandoned quarry
24	KK7A	Přední Lhota I	CSVC	leucocratic microsyenite	30	50°42.529′	14°12.031′	Dyke in quarry - centre
25	KK8	Přední Lhota II	CSVC	camptonite	30	50°42.557′	14°12.018′	Dyke in quarry
26	KK9	Svárov	RPVC	polzenite	70	50°42.313′	14°53.450′	Angular blocks
27	KK10	Velká Čertova zeď	RPVC	melilitite	70	50°40.414′	14°56.725′	Dyke exposure
28	KK11	Hamerský Špičák I	RPVC	polzenite	70	50°41.336′	14°50.989′	Angular blocks
29	KK12	Ptačí vršek	RPVC	basanite	70	50°40.509′	14°40.782′	Dyke in old quarry
30	ME-3/13	Krkavčí skála I	CSVC	nephelinite	27	50°35.150′	14°04.783′	Rock exposure
31	ME-4/13	Krkavčí skála II	CSVC	basanite	30	50°35.117′	14°04.717′	Rock exposure
32	OC-1	Veselí	RPVC	camptonite/monchiquite	30	50°38.280′	14°38.460′	Angular blocks
33	OC-2	Pelousek	RPVC	polzenite	70	50°40.680′	14°58.200′	Abandoned quarry
34	OC-9	Vesec	RPVC	polzenite	68.4	50°42.180′	14°58.980′	Angular blocks
35	OC-10	Nový Luhov	RPVC	alnöite	70	50°42.480′	14°45.000′	Angular blocks
36	OC-12	Holičský vrch	RPVC	melilitolite	70	50°40.800′	14°53.820′	Borehole

CSVC – České Středohoří Volcanic Complex; RPVC – Ralská Pahorkatina Volcanic Complex; CHB – Cheb Basin.
Ages are taken from Ulrych et al. (1998, 2002, 2013, 2014, 2018), Skala et al. (2014), Ackerman et al. (2015), Dostal et al. (2017).

(~8.6–10.8 wt.%; ~0.8–1.0 K apfu) than in mica from camptonite/monchiquite (8.8–9.4 wt.%; ~0.8–0.9 K apfu). The latter also contains mica that is relatively poor in BaO (max. 1.8 wt.% BaO). FeO^{tot} concentrations range between 6 wt.% and 10.2 wt.%, except for few dark mica analyses from polzenite that show higher contents of 14.1–15.6 wt.%. Tetrahedral Al ranges between 0.94 and 1.41 apfu along with Mg/(Mg + Fe) atomic ratio of 0.66–0.88. Dark mica from polzenite falls in the phlogopite and Mg-biotite fields, whereas dark mica from camptonite/monchiquite samples falls in the phlogopite field (Fig. 3C). Moreover, phlogopite from polzenite with very high Mg/(Mg + Fe) shows an evolutionary trend towards tetra-ferriphlogopite, which is attested by deficient tetrahedral Al in recalculated analyses (Supplement C.3).

4.3. Whole-rock geochemistry

4.3.1. Major elements

The SiO_2 and MgO contents of a representative set of 36 samples were recalculated on a volatile-free basis and range from 33 wt.% to 61 wt.% and 0.1 wt.% to 18 wt.%, respectively (Fig. 4, Table 2). The most ultrabasic rocks are Cretaceous ultramafic lamprophyres (SiO_2 ~36 wt.%) followed by associated melilitic rocks (SiO_2 ~40 wt.%). Tertiary volcanic rocks compositionally range from ultrabasic nephelinite and basic tephrite/basanite (majority of the samples with SiO_2 ~43 wt.%) to more acidic rocks of phonolite composition. Tertiary alkaline lamprophyres are basic (SiO_2 ~46 wt.%) with highly variable contents of alkalies. One sample of leucocratic microsyenite plots in the tephriphonolite field (Fig. 4).

The various samples define a coherent trend in binary variation diagrams, using SiO_2 as differentiation index, that may be interpreted as (i) fractionation trend or (ii) mixing/assimilation trend or (iii) superposition of both (Fig. 5). Generally, Al_2O_3 contents correlate positively, whereas CaO and MgO are negatively correlated. In contrast, TiO_2 contents behave differently. TiO_2 contents in Cretaceous ultramafic lamprophyres and melilitic rocks are in the range of 2–3 wt.% and correlate positively with SiO_2. Contrary to that, TiO_2 contents in the most primitive members of the Tertiary volcanic rocks and alkaline lamprophyres reach ~4 wt.% and correlate negatively with increasing SiO_2. FeO^{tot} behaves similarly as TiO_2 (Fig. 5). K_2O contents are ~2 wt.% in the majority of ultramafic lamprophyres and associated melilitic rocks. In the most primitive members of Tertiary volcanic samples, K_2O contents are below 1.5 wt.% and correlate positively with increasing SiO_2. An extremely high K_2O content of 8.3 wt.% was found in a leucocratic microsyenite (sample KK7A).

4.3.2. Trace elements

The samples generally have highly variable transition metal contents and a slightly variable enrichment of large-ion lithophile elements (LILE) and light rare earth elements (LREE) relative to high-field strength elements (HFSE) and heavy rare earth elements (HREE). This is clearly visible both in binary variation diagrams and in primitive mantle normalised trace and chondrite normalised rare earth element abundance plots (Figs. 5 and 6A–F).

The highest Cr concentrations (up to 800 ppm) occur in Cretaceous ultramafic lamprophyres and associated melilitic rocks. Chromium correlates negatively with increasing SiO_2, reaching levels as low as 2 ppm Cr in differentiated trachyte (Fig. 5, Table 2). Cretaceous ultramafic lamprophyres show the highest degree of LREE enrichment. La, Ce and Ce/Yb show a negative correlation with increasing SiO_2 for ultramafic

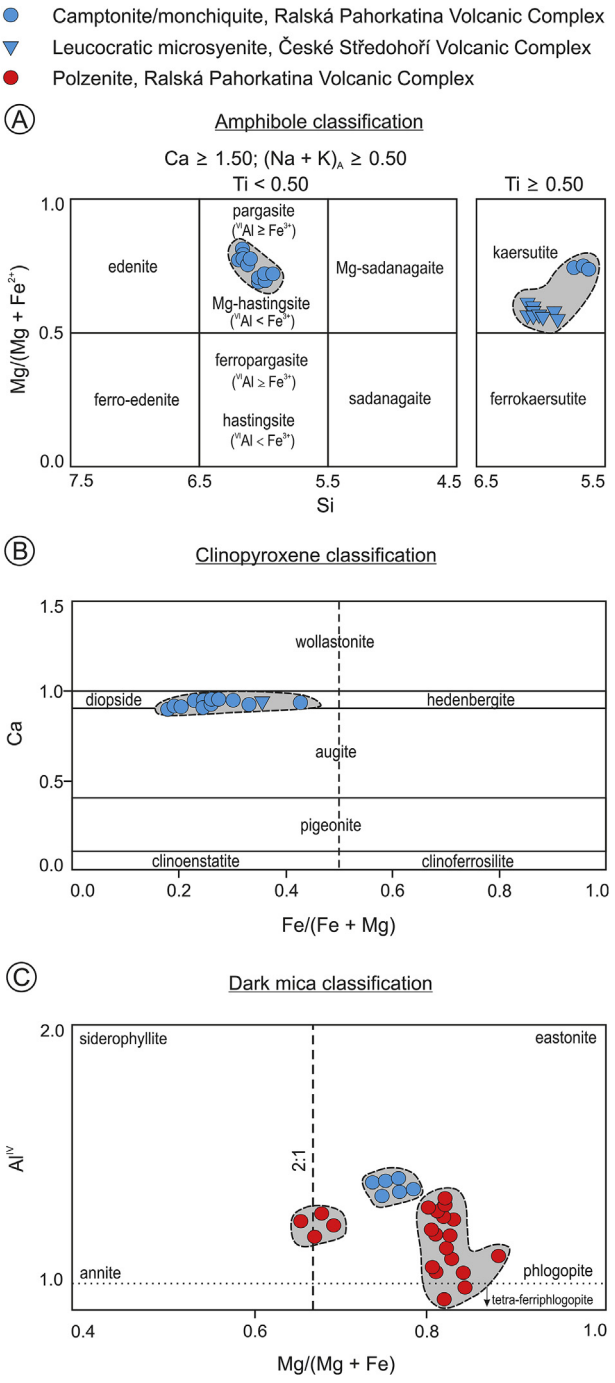

Fig. 3. Classification of amphibole, clinopyroxene and dark mica from camptonite/monchiquite, leucocratic microsyenite, and polzenite. All chemical elements are given in apfu (atoms per formula unit). (A) Analyses of amphibole phenocrysts from camptonite/monchiquite samples plot in the fields of both pargasite and kaersutite, whereas amphibole in leucocratic microsyenite falls in the kaersutite field of the amphibole classification scheme of Leake (1997). (B) Clinopyroxene from both camptonite/monchiquite and leucocratic microsyenite samples is diopside (Morimoto, 1988), diagram adopted from Rapprich (2005). (C) Dark mica from camptonite/monchiquite and polzenite corresponds to phlogopite. Dark mica from camptonite/monchiquite is compositionally rather homogeneous, whereas dark mica from polzenite falls in two groups ranging from phlogopite to Mg-biotite. Classification diagram after Rieder et al. (1998).

lamprophyres towards tephritic and basanitc rocks (Fig. 5).

The Cretaceous ultramafic lamprophyres and associated melilitic rocks are characterised by troughs for K and Pb in primitive mantle

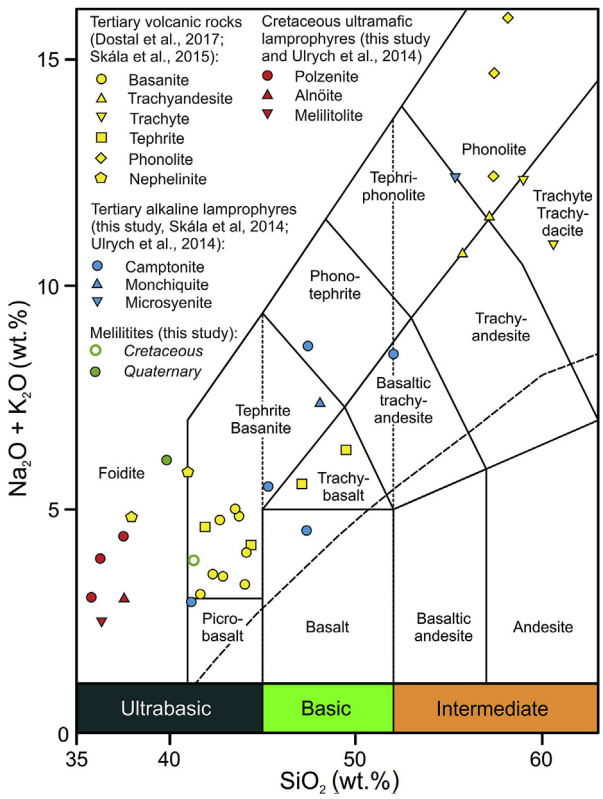

Fig. 4. Total Alkali-Silica (TAS) diagram showing the chemical composition of analysed samples (after Le Maitre, 2002).

normalised trace element plots (Fig. 6A). Tertiary alkaline lamprophyres show slightly negative or even positive anomalies for K along with Pb enrichment and P depletion. The leucocratic microsyenite has the most pronounced anomalies among the analysed alkaline lamprophyres and related rocks (Fig. 6C). Absolute trace element concentrations in Tertiary volcanic samples differ from those of the basanite/tephrite samples and the more evolved trachytic/phonolitic samples. However, they define the same trends in primitive mantle normalised trace element plots. Tertiary volcanic samples show variable Rb depletion, K and Pb depletion or enrichment, as well as troughs for P and Ti that markedly increase from basanite/tephrite to trachyte/phonolite samples (Fig. 6E). There are two geochemical types of phonolite in the representative sample set: type A (Sr-rich) and type B (Sr-poor), first characterised by Ackerman et al. (2015). Whereas the samples of type A phonolite compositionally resemble other types of evolved volcanic rocks, type B phonolite is prominent by extreme depletion of Ba, Sr, P, and Ti along the most pronounced Cs, U, and Pb enrichments among all Tertiary volcanic rocks (Fig. 6E).

The samples show variable REE contents and generally lack pronounced Eu anomalies (Fig. 6B, D, F). Cretaceous ultramafic lamprophyres have the highest total REE contents (ΣREE ~500 ppm), whereas Tertiary trachytic/phonolitic samples have the lowest total REE contents of ~270 ppm. Ultramafic lamprophyres together with associated melilitic samples are prominent by the highest enrichment in LREE over HREE with Ce_N/Yb_N of ~30 and Lu_N of ~7, whereas Tertiary volcanic samples have contrasting enrichment trends in LREE/HREE (Ce_N/Yb_N ~21 in basanite/tephrite samples, and ~31 in more differentiated trachyte/phonolite samples). Type B phonolite is prominent by its U-shaped REE normalised pattern (Fig. 6F). Ultramafic lamprophyres, associated melilitic rocks, the majority of alkaline lamprophyres and basanite/tephrite volcanic rocks all have $Lu_N < 10$ indicating the presence of garnet in the mantle source of their parent melts (see Wilson and Downes, 1991).

Table 2
Major oxide (wt.%) and trace element compositions (ppm) of mantle-derived rocks of the Bohemian Massif.

No.	1[a]	2[a]	3[a]	4[a]	5[a]	6[a]	7[a]	8[a]	9[a]	10[a]	11[a]	12[a]	13[a]	14[a]	15[b]	16[b]
Sample	1_1367	4_New	5_New	8_1299	12_1295	14_1358	15_1359	17_BM-8	18_BM-16	19_BM-48	20_BM-13	21_BM-51	23_BM-4	25_BM-60	CS-30	CS-31
SiO_2	40.2	40.4	42.3	41.6	47.0	45.2	42.2	55.8	55.2	54.2	59.1	56.8	53.9	54.6	45.9	47.8
TiO_2	2.65	3.73	3.3	2.8	2.97	3.59	3.92	0.14	0.59	0.28	0.57	0.45	1.27	0.86	3.22	2.13
Al_2O_3	11.1	12.1	14.7	13.5	15.2	15.5	13.6	21.4	20.3	21.7	19.8	20.2	18.9	19.7	15.0	16.2
$Fe_2O_3^{tot}$	12.5	14.0	12.1	11.5	9.6	10.8	11.5	2.3	3.63	2.2	3.22	3.11	5.66	4.36	11.1	8.34
MnO	0.19	0.19	0.19	0.19	0.16	0.18	0.33	0.28	0.23	0.26	0.23	0.22	0.2	0.2	0.16	0.16
MgO	12.9	8.91	8.4	9.87	4.57	5.4	6.53	0.08	0.43	0.23	0.21	0.34	1.32	0.67	4.91	2.48
CaO	12.5	12.5	11.8	12.6	9.85	10.6	13.5	0.95	4.15	1.8	3.4	3.59	5.4	4.42	8.79	7.35
Na_2O	2.73	1.85	2.25	1.84	3.67	3.38	2.61	9.9	6.85	9.11	5.0	6.47	6.47	5.94	2.92	3.7
K_2O	0.66	1.47	1.63	1.31	2.31	1.96	1.38	5.46	5.05	4.73	5.69	5.39	3.84	5.06	4.09	4.07
P_2O_5	0.79	0.68	0.54	0.54	0.49	0.51	0.65	0.02	0.1	0.03	0.08	0.07	0.35	0.15	0.47	0.52
LOI	2.61	3.2	2.69	2.99	3.62	3.27	4.31	1.79	2.16	5.52	2.47	3.22	2.77	4.51	3.44	6.86
Total	98.8	99.1	99.9	98.7	99.4	100.4	100.5	98.2	98.7	100.1	99.8	99.8	100.1	100.5	99.9	99.6
Mg#	67	56	58	63	49	50	53	6	19	17	11	18	32	23	47	37
Cr	350	210	140	320	50	40	70	10	10	2	2	10	20	10	27	16
Ni	280	170	120	190	10	70	90	10	10	10	10	10	20	10	22	15
Co	51	45	40	44	26	30	34	1	14	4	5	7	14	7	31	17
Sc	26	29	30	32	20	24	30	1	1	1	0	0	4	1	24	10
V	281	336	345	317	336	378	436	23	71	18	60	57	108	100	367	212
Cu	70	60	70	90	40	60	180	5	10	5	5	5	10	5	–	–
Zn	110	110	100	100	90	110	120	150	130	175	118	110	130	120	–	–
Rb	10	36	33	29	144	84	44	371	123	219	184	153	98	121	81	117
Cs	0.5	0.5	0.0	1.7	1.7	1.4	1.2	9.9	1.4	4.78	5.45	2.0	1.70	2.5	0.9	1.5
Ba	643	600	494	700	992	776	752	17	1880	620	1870	1730	1400	1420	781	937
Sr	981	1260	1290	1000	937	904	1070	21	2070	433	1830	1560	1570	1410	641	1000
Ga	18	19	19	18	20	24	24	53	27	25	41	27	29	26	–	–
Ta	4.6	7.1	4.5	5.7	4.4	5.5	5.7	2.02	5.5	7.2	8.56	4.1	6.9	5.0	4.84	6.13
Nb	68	70	66	79	70	78	76	138	140	447	198	113	127	110	94	123
Hf	5.0	6.2	8.0	5.3	6.7	8.1	7.9	21.2	10.2	22.2	11.1	10.0	13.1	10.4	9.2	12.4
Zr	228	232	211	218	324	329	323	1200	543	1650	634	568	615	562	359	576
Y	23	27	22	22	22	22	24	16	24	24	29	20	27	22	21	25
Pb	4	4	3	4	7	7	7	34	9	12	25	11	15	11	6	7
Th	7.5	4.2	5.0	6.5	7.9	8.9	9.0	49.7	14.8	28.8	15.4	15.3	17.9	14.6	8.9	11.8
U	1.9	1.1	1.4	1.6	2.3	3.1	5.7	18.6	3.8	16.6	4.0	3.9	4.1	3.4	2.0	3.4
La	68	46	44	60	58	51	69	139	124	115	148	112	108	110	49	77
Ce	124	96.7	87.7	112	112	105	133	146	210	160	216	178	186	181	101	147
Pr	13.7	12.3	10.3	12.3	12.9	12.4	15.4	8.5	19.5	22.0	13.0	15.9	18.7	17.6	11.8	16.4
Nd	50.2	49.2	39.4	43.8	48.2	47.4	57.6	17.3	56.1	45.8	67.3	44.0	60.9	54.4	45.8	59.3
Sm	9.2	10.1	7.5	7.9	8.6	8.5	10.4	1.61	6.8	6.72	8.2	5.6	9.3	7.5	8.58	9.84
Eu	2.92	3.21	2.35	2.5	2.49	2.53	3.08	0.32	2.01	1.34	2.06	1.56	2.71	2.18	2.48	2.89
Gd	7.7	8.4	6.3	6.5	6.5	6.5	8.2	1.13	4.9	3.9	4.4	3.7	6.9	5.4	8.21	9.88
Tb	1.0	1.2	0.9	0.9	0.9	0.9	1.1	0.22	0.7	0.69	0.8	0.5	0.9	0.7	1.03	1.23
Dy	5.1	5.8	4.7	4.8	4.6	4.6	5.3	1.56	3.7	5.3	5.7	3.0	5.0	3.9	4.84	5.62
Ho	0.9	1.0	0.9	0.9	0.8	0.8	0.9	0.41	0.7	0.9	0.9	0.6	0.9	0.8	0.85	1.0
Er	2.3	2.6	2.2	2.3	2.2	2.2	2.3	1.6	2.4	2.8	2.8	2.0	2.7	2.2	2.35	2.88
Tm	0.3	0.34	0.29	0.29	0.29	0.3	0.32	0.34	0.36	0.45	0.52	0.32	0.39	0.33	0.28	0.36
Yb	1.8	1.9	1.9	1.8	1.9	1.8	1.8	2.98	2.4	3.94	2.88	2.3	2.6	2.2	1.81	2.37
Lu	0.25	0.26	0.28	0.27	0.28	0.26	0.26	0.52	0.4	0.61	0.48	0.37	0.41	0.35	0.27	0.34

No.	17[b]	18	19	20	21	22	23	24	25	26	27	28	29	30[c]	31[c]	32[d]	33[d]	34[d]	35[d]	36[d]
Sample	CS-43	KK1	KK2	KK3	KK4	KK5	KK6	KK7A	KK8	KK9	KK10	KK11	KK12	ME-3/13	ME-4/13	OC-1	OC-2	OC-9	OC-10	OC-12
SiO_2	42.7	38.2	39.2	42.4	41.7	40.6	44.9	52.8	45.2	33.8	39.9	33.1	41.3	36.8	39.9	38.9	34.0	30.6	34.1	31.5
TiO_2	2.97	3.1	3.4	3.17	3.73	3.22	2.62	1.45	3.25	2.62	2.96	2.47	3.08	3.07	2.63	3.43	2.57	2.28	2.1	2.57
Al_2O_3	13.8	11.5	11.8	13.6	14.5	14.7	13.0	17.8	15.8	7.88	9.99	7.74	14.5	12.6	12.2	13.7	8.96	7.38	8.24	8.65

(*continued on next page*)

Table 2 (*continued*)

No.	17[b]	18	19	20	21	22	23	24	25	26	27	28	29	30[c]	31[c]	32[d]	33[d]	34[d]	35[d]	36[d]
Sample	CS-43	KK1	KK2	KK3	KK4	KK5	KK6	KK7A	KK8	KK9	KK10	KK11	KK12	ME-3/13	ME-4/13	OC-1	OC-2	OC-9	OC-10	OC-12
$Fe_2O_3^{tot}$	11.6	13.2	15.6	12.4	12.5	13.3	11.9	5.58	10.4	11.7	11.5	10.8	13.0	13.6	12.9	12.3	12.1	11.6	13.7	10.7
MnO	0.19	0.23	0.33	0.18	0.2	0.22	0.23	0.15	0.17	0.2	0.18	0.19	0.21	0.22	0.18	0.16	0.2	0.2	0.2	0.17
MgO	7.88	12.1	7.15	9.15	7.07	8.36	5.94	1.79	4.71	15.3	15.7	16.9	7.90	11.4	13.6	11.0	15.1	17.0	16.5	13.4
CaO	10.5	12.4	12.0	12.0	11.8	12.4	11.8	4.28	8.07	16.1	13.0	18.6	12.7	14.7	12.1	13.2	14.1	21.1	16.4	17.9
Na_2O	3.03	3.71	4.39	3.13	3.03	2.92	2.62	3.79	4.03	1.02	2.31	1.59	3.3	3.19	2.02	0.89	2.16	0.52	2.01	0.22
K_2O	2.15	2.15	1.1	1.57	1.75	1.53	1.67	7.97	4.17	1.72	1.41	1.25	1.33	1.5	0.96	1.9	1.85	0.75	1.66	1.98
P_2O_5	0.6	0.92	1.41	0.73	0.77	1.09	1.23	0.32	0.52	1.24	0.75	1.30	0.87	1.5	0.63	0.53	1.07	1.12	1.09	0.95
LOI	4.57	1.8	3.0	1.1	2.3	1.2	3.6	3.7	3.2	7.6	1.4	5.2	1.4	1.8	3.5	5.18	7.4	6.3	4.9	12.0
Total	100.0	99.4	99.3	99.4	99.4	99.5	99.5	99.6	99.5	99.2	99.2	99.2	99.5	100.4	100.6	101.1	99.6	98.8	100.4	100.0
Mg#	57	65	48	59	53	56	50	39	47	72	73	76	55	63	68	64	71	74	71	71
Cr	70	431	27	294	144	130	55	14	34	602	842	746	192	197	486	262	749	810	623	700
Ni	75	147	25	98	41	54	27	5	12	317	339	336	56	132	239	134	327	330	253	216
Co	37	56	37	46	40	43	31	9	28	53	59	60	43	55	60	51	56	59	61	47
Sc	30	29	21	27	26	27	17	5	20	22	30	26	24	27	31	45	33	23	30	22
V	345	304	275	289	348	336	269	141	341	252	308	210	315	378	334	–	–	252	–	–
Cu	–	48	38	70	61	47	38	9	46	52	76	48	56	–	–	–	–	30	–	–
Zn	–	63	150	90	100	88	91	77	82	86	72	65	84	–	–	–	–	70	–	–
Rb	38	54	21	35	64	37	48	222	118	49	51	47	32	29	35	154	64	26	48	65
Cs	1.3	0.4	1.0	0.4	0.6	0.2	1.2	1.80	1.2	0.9	1.0	0.8	0.4	0.8	0.5	1.89	2.9	0.5	0.93	3.03
Ba	654	965	1030	717	791	591	541	1070	868	737	807	968	726	1470	651	1610	1980	717	1380	754
Sr	920	807	1580	937	1700	940	1230	757	890	866	873	1420	1140	1770	963	854	2000	1800	1780	1280
Ga	–	21	25	19	22	20	17	21	21	13	14	12	19	–	–	–	–	18	–	–
Ta	4.9	6.8	10.1	4.5	4.8	5.7	5.7	5.2	5.1	8.5	5.1	6.9	5.3	5.8	4.1	3.49	5.5	10.7	7.80	7.73
Nb	95	122	168	87	78	88	96	107	82	129	84	134	90	141	96	79	188	151	183	125
Hf	8.1	6.7	14.7	5.8	8.2	6.3	7.0	9.7	8.2	5.5	5.7	4.6	6.1	8.5	7.1	10.2	7.5	5.5	6.3	7.8
Zr	313	299	616	233	351	256	290	461	340	251	224	197	243	333	259	301	357	247	292	345
Y	24	27	42	25	29	28	30	23	23	30	19	24	27	34	21	21	26	29	28	29
Pb	17	2	5	6	4	2	4	15	8	5	3	4	2	10	3	4	6	4	6	4
Th	7.6	11.3	13.8	6.9	6.6	7.1	8.0	18.4	10.0	16.1	6.4	12.7	6.9	17.0	7.0	12.3	15.0	23.0	17.0	10.2
U	2.1	3.1	3.9	1.5	1.8	1.6	2.0	5.2	2.5	3.9	1.6	2.9	1.5	3.7	1.7	1.45	3.9	4.83	4.8	2.49
La	62	89	125	58	63	67	73	80	57	124	52	106	62	165	64	51	103	163	130	84
Ce	128	168	249	110	132	136	144	145	115	248	104	201	125	289	117	104	186	304	235	177
Pr	14.6	18.9	28.7	12.1	15.4	15.4	16.9	14.8	13.0	28.2	11.9	22.2	14.7	28.0	13.0	12.5	21.0	33.8	25.0	19.9
Nd	56.9	69.3	110	46.1	61.5	59.6	61.5	50.4	50.4	106	46.1	84.3	56.9	102	48.0	50.6	79.0	120	90.0	77.2
Sm	10.3	11.4	18.0	8.5	11.0	10.7	10.4	7.69	8.4	17.1	8.61	13.9	9.67	16.0	8.4	9.27	13.0	18.4	14.0	13.4
Eu	3.02	3.33	5.01	2.52	3.3	3.11	3.13	2.06	2.42	4.73	2.56	3.92	3.07	4.5	2.5	2.74	3.6	5.13	3.9	3.85
Gd	9.74	9.34	14.2	7.51	9.39	8.98	9.05	6.11	6.97	12.7	7.06	10.6	8.29	15.0	8.1	8.61	10.0	12.9	13.0	13.9
Tb	1.22	1.16	1.75	0.98	1.2	1.11	1.16	0.83	0.9	1.52	0.86	1.23	1.08	1.7	1.0	1.03	1.30	1.53	1.5	1.62
Dy	5.51	5.88	8.98	5.13	6.31	6.35	6.50	4.58	4.93	7.69	4.28	6.03	5.88	7.6	4.8	4.77	6.6	7.08	6.3	6.28
Ho	0.96	0.95	1.52	0.88	1.02	1.04	1.07	0.75	0.84	1.12	0.67	0.91	0.94	1.3	0.85	0.82	1.10	1.11	1.0	0.97
Er	2.72	2.46	3.93	2.29	2.83	2.86	2.83	2.31	2.28	2.66	1.67	2.18	2.53	3.6	2.3	2.19	2.6	2.61	2.6	2.87
Tm	0.33	0.31	0.56	0.28	0.35	0.38	0.37	0.32	0.31	0.32	0.19	0.25	0.33	0.42	0.27	0.26	0.33	0.3	0.3	0.29
Yb	2.05	1.89	3.33	1.89	2.16	2.15	2.46	2.30	1.94	1.84	1.26	1.49	1.92	2.6	1.7	1.92	1.9	1.63	1.8	1.82
Lu	0.29	0.26	0.49	0.25	0.33	0.34	0.35	0.33	0.3	0.25	0.16	0.19	0.29	0.36	0.23	0.22	0.25	0.21	0.23	0.25

LOI - loss on ignition; Mg# = 100 × Mg/(Mg + Fe^{tot}).

[a] Analyses adopted from Dostal et al. (2017).

[b] Analyses adopted from Skála et al. (2014).

[c] Analyses adopted from Skála et al. (2015).

[d] Analyses adopted from Ulrych et al. (2014).

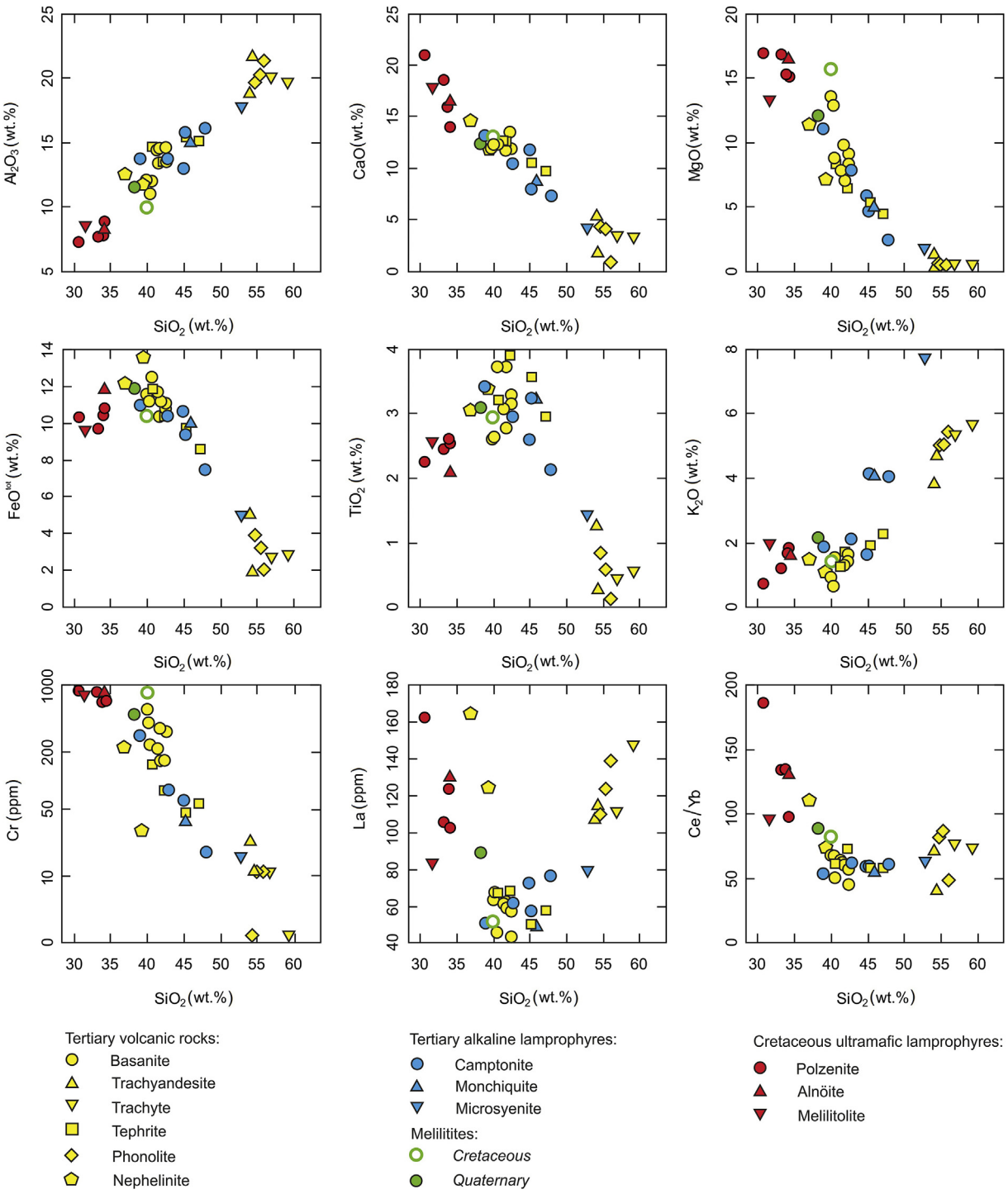

Fig. 5. SiO_2 *vs.* selected major and trace element contents of analysed samples.

4.4. *Lead isotope composition*

The initial lead isotope composition of Cretaceous ultramafic lamprophyres, Tertiary basaltic volcanic samples as well as alkaline lamprophyres, related leucocratic microsyenite and Cretaceous and Quaternary melilitite rocks defines a scattered linear trend between two end-members (schematically marked by red asterisks A and B in Figs. 7, 9 and 10). In the $^{207}Pb/^{204}Pb$ vs. $^{206}Pb/^{204}Pb$ diagram, most data fall above the Northern Hemisphere Reference Line (NHRL; Hart, 1984), whereas in the $^{208}Pb/^{204}Pb$ vs. $^{206}Pb/^{204}Pb$ diagram, the Pb trend intersects the NHRL, as it is slightly flatter than the NHRL (Fig. 7).

The Cretaceous ultramafic lamprophyres and melilitolite sample of the RPVC sampled a more radiogenic mantle component ($^{206}Pb/^{204}Pb$ = 19.62–20.01, $^{207}Pb/^{204}Pb$ = 15.61–15.64, $^{208}Pb/^{204}Pb$ = 39.29–39.77) than the Tertiary alkaline lamprophyres and associated leucocratic microsyenite ($^{206}Pb/^{204}Pb$ = 19.05–19.35, $^{207}Pb/^{204}Pb$ = 15.60–15.61, $^{208}Pb/^{204}Pb$ = 38.91–39.14; Table 3). The Cenozoic volcanic samples have a very heterogeneous Pb isotope composition ($^{206}Pb/^{204}Pb$ = 18.98–19.96, $^{207}Pb/^{204}Pb$ = 15.59–15.65, $^{208}Pb/^{204}Pb$ = 38.80–39.62). Data points plot along a linear array extending from the least radiogenic Pb isotope compositions of the alkaline lamprophyres to the most radiogenic compositions of the ultramafic lamprophyres (Fig. 7).

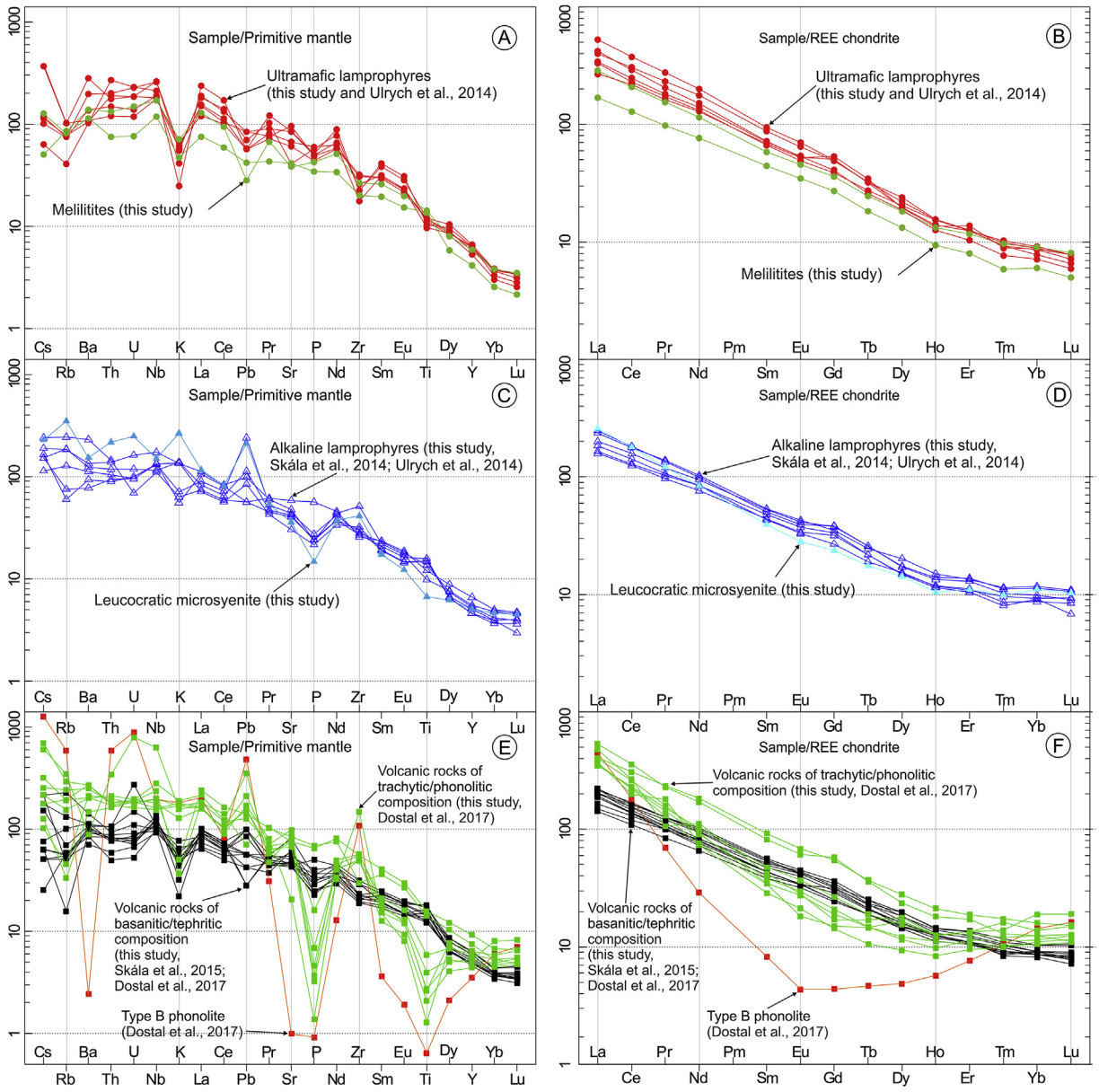

Fig. 6. Abundances of trace elements and rare earth elements (REE) in the analysed samples normalised to primitive mantle values (McDonough and Sun, 1995) and chondritic abundances (Boynton, 1984), respectively.

Intrusive and effusive melilitite samples, which are of Cretaceous and Quaternary age, respectively, have essentially identical Pb isotope compositions ($^{206}Pb/^{204}Pb$ = 19.30–19.36, $^{207}Pb/^{204}Pb$ = 15.60, $^{208}Pb/^{204}Pb$ = 39.09–39.10).

Among the ultramafic lamprophyres, alnöite OC-10 with a $^{206}Pb/^{204}Pb$ ratio of 20.01 is the most radiogenic sample and melilitolite OC-12 with $^{206}Pb/^{204}Pb$ ratio of 19.62 is the least radiogenic sample. The Pb isotope compositions of polzenite samples fall between these two values (Fig. 7). The monchiquites from the CSVC as well as the camptonite to monchiquite sample OC-1 are among the least radiogenic samples from the Bohemian Massif. They have $^{206}Pb/^{204}Pb$ ratios of 19.05–19.10. Similarly, the Pb isotope signature of the leucocratic microsyenite is very unradiogenic and points to derivation from the same mantle source as the less fractionated camptonites and monchiquites.

5. Discussion

5.1. Chemically contrasting mantle sources in the Bohemian Massif

Common K-bearing silicate phases such as phlogopite or K-amphibole are not stable in the asthenospheric (convective) mantle (Class and Goldstein, 1997). Negative K anomalies observed in intraplate mantle-derived rocks indicate that these phases were stable during the petrogenesis of these rocks, and, thus, are considered as geochemical evidence for the involvement of lithospheric mantle sources (e.g., Wilson and Downes, 1992; Melluso et al., 2011; Pfänder et al., 2018).

Variations in the whole-rock composition of Late Cretaceous to Quaternary undifferentiated magmatic rocks from the Bohemian Massif point to contributions from two geochemically distinct mantle sources. The Cretaceous ultramafic lamprophyres show strong LREE over HREE enrichment (Fig. 6B) in combination with high K_2O and low TiO_2 at given SiO_2 (Fig. 5) and significant troughs in K and Pb in primitive mantle

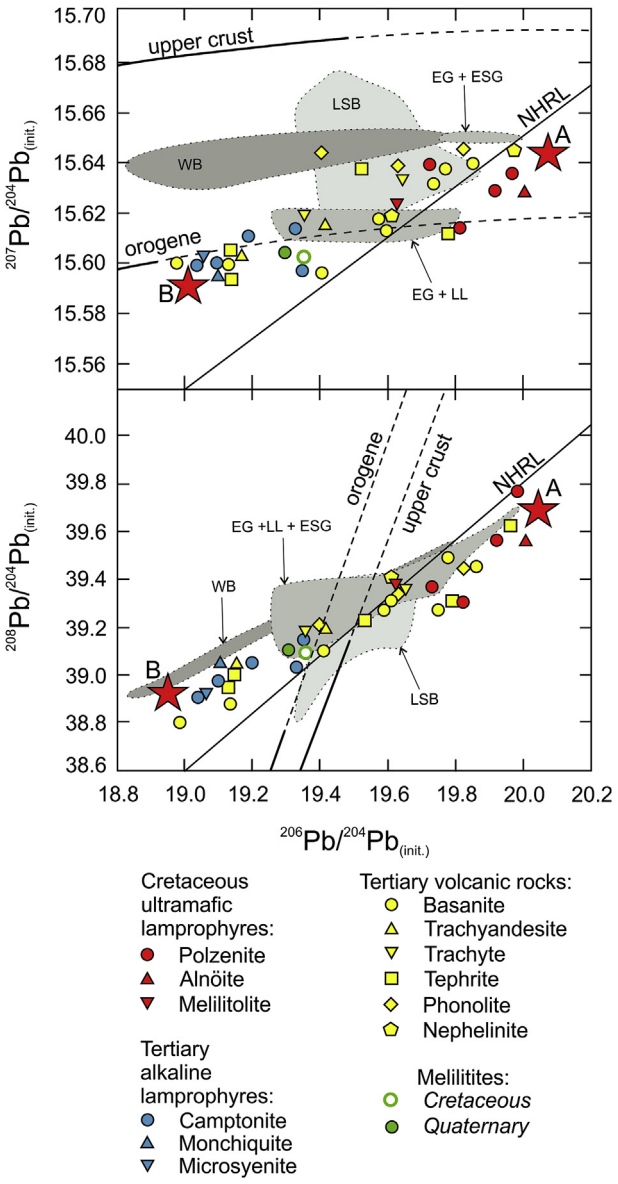

Fig. 7. Initial Pb isotope composition of individual samples from the Bohemian Massif. Melilitite samples of different age (Cretaceous and Quaternary) are plotted separately as their Pb isotope composition is relatively uniform but different from other melilitic rocks (i.e., ultramafic lamprophyres). NHRL: Northern Hemisphere Reference Line (Hart, 1984). Abbreviations and references for other volcanic fields from the Bohemian Massif: WB – Western Bohemia (Ulrych et al., 2016); LSB – Lower Silesian Basin (Blusztajn and Hart, 1989); EG – Erzgebirge, ESG – Elbsandsteingebirge, LL – Lower Lusatia (Haase and Renno, 2008).

normalised trace element plots (Fig. 6A), indicating that they originated by low degrees of partial melting of a metasomatised lithospheric mantle source containing a stable K-bearing residual phase (e.g., Ulrych et al., 2008, 2014; Skála et al., 2015). Such a lithospheric mantle formed during Variscan subduction of continental crust. This process led to stabilization of metasomatised parts containing inclusions of granitic composition within the mantle rocks beneath the Saxothuringian and Moldanubian zones of the Bohemian Massif (Borghini et al., 2018; Ferrero et al., 2018 and references therein). This is in line with the composition of phlogopite in ultramafic lamprophyres that shows high MgO and elevated K_2O and BaO contents, coupled with a compositional affinity towards the tetra-ferriphlogopite end-member (cf. Skála et al., 2015). Moreover, K-rich sulphides of rasvumite (KFe_2S_3) type, identified by Ulrych et al. (2008), occur locally in association with phlogopite in melilitolites. Such a K-rich sulphide may be a primary phase that crystallised from metasomatised lithospheric mantle-derived ultramafic melts (e.g., Sharygin et al., 2008).

Compared with the source of Cretaceous ultramafic lamprophyres, the second mantle source is characterised by significant TiO_2 enrichment and K_2O depletion. This resulted in relatively flat OIB-like primitive mantle normalised trace element patterns for the majority of the Tertiary alkaline lamprophyres (characterised by the presence of TiO_2-rich amphibole – kaersutite with up to 0.74 apfu Ti) and basanite/tephrite volcanic rocks (Fig. 6C, E). Their mantle source was significantly influenced by interaction with asthenospheric (convective) mantle depleted in large-ion lithophile elements (Rock, 1991). This is in line with rift-related passive asthenospheric upwelling that resulted in the generation of large volumes of Tertiary mantle-derived magmas in the Eger Rift (e.g., Ulrych et al., 2011).

Both mantle sources are distinguishable: undifferentiated Cretaceous ultramafic lamprophyres show a trend with relatively large variations in Nb/Ta and narrow variation in Lu/Hf, whereas Tertiary alkaline lamprophyres and basanite/tephrite volcanic rocks show a narrow range of Nb/Ta values as also known from OIB's (Fig. 8A). The higher and more variable Nb/Ta ratios in the Cretaceous ultramafic lamprophyres likely indicate a higher contribution from the lithospheric mantle and a more heterogeneous source than for the Tertiary alkaline lamprophyres and the basanite/tephrite volcanic rocks (cf. Pfänder et al., 2012). The Cretaceous ultramafic lamprophyres and undifferentiated Cenozoic volcanic rocks show a comparable range in Nb/La ratios at different $(Ce/Yb)_N$ (Fig. 8B). The Nb/La ratios fall between the values for depleted MORB mantle source and for the lithospheric mantle source metasomatised by continental crust (Fig. 8B). The narrow range of Nb/La ratios may be indicative for a similarly enriched mantle source, whereas different $(Ce/Yb)_N$ may reflect contrasting degrees of partial melting (cf. Haase and Renno, 2008). The Cretaceous ultramafic lamprophyres and undifferentiated Cenozoic volcanic rocks show different trends in the Ba/La *vs.* $(Ce/Yb)_N$ diagram (Fig. 8C), which may indicate involvement of different mantle sources. For instance, the high and variable $(Ce/Yb)_N$ and relatively constant Ba/La ratios of Cretaceous ultramafic lamprophyres may reflect different degrees of partial melting of highly metasomatised domains of the lithospheric mantle, producing such SiO_2-undersaturated melts (cf. Hegner et al., 1995; Blusztajn and Hegner, 2002). In contrast, Cenozoic volcanic rocks with relatively constant $(Ce/Yb)_N$ and highly variable Ba/La may reflect a carbonatite component (Haase et al., 2017), which may be indicative for a mantle source that was affected by interaction with the convective mantle. Significant CO_2 release from the asthenosphere in a continental rifting environment is also indicated by metasomatised mantle xenoliths from the lithospheric mantle beneath the Bohemian Massif (Ackerman et al., 2013). Besides these compositional differences related to different degrees of partial melting of heterogeneously metasomatised mantle sources, fractional crystallisation also affected the chemical composition of the rocks (Dostal et al., 2017). Fractional crystallisation in particular affected the composition of Tertiary trachytic to phonolitic volcanic rocks and the leucocratic microsyenite of the CSVC and is reflected in linear enrichment trends for SiO_2, Al_2O_3 and K_2O and depletion trends for CaO, MgO, FeO^{tot}, Cr_2O_3, P_2O_5 or TiO_2 (Figs. 5 and 6).

5.2. *Lead isotope compositions of the samples – asthenospheric vs. lithospheric mantle components*

The lead isotope data define a relatively narrow two-component mixing trend ranging from moderately high $^{206}Pb/^{204}Pb$ ratios (~19.0) to more radiogenic values (up to 20.0), suggesting a mixture between a mantle source showing geochemical characteristics of modification by interaction with convective mantle and metasomatically enriched lithospheric mantle (cf. Blusztajn and Hart, 1989; Stracke et al., 2005; Ulrych et al., 2016 and section 5.1 in this paper). The suggested two-component

Table 3
Whole-rock Pb isotope data of the mantle-derived rocks of the Bohemian Massif.

No.	Sample	Area	Rock type	Age (Ma)	$^{206}Pb/^{204}Pb$	$^{207}Pb/^{204}Pb$	$^{208}Pb/^{204}Pb$	$^{206}Pb/^{204}Pb$ (T)	$^{207}Pb/^{204}Pb$ (T)	$^{208}Pb/^{204}Pb$ (T)
1	1_1367	CSVC	basanite	41.9	19.752	15.620	39.489	19.55	15.61	39.23
2	4_New	CSVC	basanite	30	19.218	15.604	38.983	19.14	15.60	38.88
3	5_New	CSVC	basanite	30	20.001	15.647	39.619	19.86	15.64	39.45
4	8_1299	CSVC	basanite	25.4	19.902	15.644	39.652	19.80	15.64	39.51
5	12_1295	CSVC	trachybasalt	26.8	19.222	15.599	39.060	19.13	15.59	38.96
6	14_1358	CSVC	trachybasalt	24.7	19.280	15.610	39.127	19.17	15.60	39.02
7	15_1359	CSVC	tephrite	26.6	19.781	15.650	39.356	19.56	15.64	39.24
8	17_BM-8	CSVC	phonolite	25.8	19.577	15.652	39.343	19.43	15.65	39.22
9	18_BM-16	CSVC	phonolite	30	19.763	15.645	39.510	19.63	15.64	39.34
10	19_BM-48	CSVC	phonolite	30	20.021	15.655	39.551	19.83	15.65	39.44
11	20_BM-13	CSVC	trachyte	30	19.426	15.623	39.270	19.36	15.62	39.18
12	21_BM-51	CSVC	trachyte	30	19.756	15.639	39.497	19.65	15.63	39.36
13	23_BM-4	CSVC	trachyandesite	31	19.237	15.607	39.164	19.15	15.60	39.04
14	25_BM-60	CSVC	trachyandesite	30	19.509	15.620	39.324	19.41	15.62	39.19
15	CS-30	CSVC	monchiquite	30	19.201	15.601	39.187	19.10	15.60	39.04
16	CS-31	CSVC	camptonite	30	19.345	15.618	39.216	19.20	15.61	39.05
17	CS-43	CSVC	camptonite	30	19.389	15.600	39.190	19.35	15.60	39.14
18	KK1	CHB	melilitite	1	19.323	15.605	39.119	19.30	15.60	39.10
19	KK2	CSVC	tephrite	25.6	20.178	15.655	39.873	19.97	15.65	39.63
20	KK3	CSVC	bazanite	29.7	19.057	15.604	38.908	18.98	15.60	38.79
21	KK4	RPVC	bazanite	30	19.542	15.603	39.259	19.41	15.60	39.10
22	KK5	RPVC	tephrite	30	20.041	15.625	39.665	19.79	15.61	39.31
23	KK6	RPVC	camptonite	28.7	19.493	15.622	39.244	19.35	15.62	39.05
24	KK7A	CSVC	microsyenite	30	19.161	15.608	39.039	19.06	15.60	38.92
25	KK8	CSVC	camptonite	30	19.193	15.603	39.088	19.10	15.60	38.97
26	KK9	RPVC	polzenite	70	20.309	15.667	40.152	19.73	15.64	39.37
27	KK10	RPVC	melilitite	70	19.756	15.622	39.613	19.36	15.60	39.09
28	KK11	RPVC	polzenite	70	20.422	15.644	40.173	19.82	15.61	39.30
29	KK12	RPVC	basanite	70	19.988	15.644	39.634	19.74	15.63	39.29
30	ME-3/13	CSVC	nephelinite	27	19.720	15.625	39.536	19.62	15.62	39.38
31	ME-4/13	CSVC	basanite	30	19.743	15.626	39.481	19.59	15.62	39.27
32	OC-1	RPVC	camptonite	30	19.164	15.606	39.067	19.05	15.60	38.91
33	OC-2	RPVC	polzenite	70	20.491	15.656	40.210	19.92	15.63	39.56
34	OC-9	RPVC	polzenite	68.4	20.849	15.678	41.135	19.97	15.64	39.77
35	OC-10	RPVC	alnöite	70	20.567	15.655	40.233	20.01	15.63	39.55
36	OC-12	RPVC	melilitolite	70	19.951	15.638	39.816	19.62	15.62	39.38

T – Lead isotope data recalculated for their published age using the constants recommended by IUGS ($\lambda^{232}Th = 4.9475E{-}11^{y-1}$, $\lambda^{235}U = 9.8485E{-}10^{y-1}$, $\lambda^{238}U = 1.55125E{-}10^{y-1}$), and Pb, U and Th concentrations listed in Table 2.
Ages are taken from Ulrych et al. (1998, 2002, 2013, 2014, 2018), Skala et al. (2014), Ackerman et al. (2015), Dostal et al. (2017).

mixing trend crosses the NHRL of Hart (1984) and most samples have higher $^{207}Pb/^{204}$ Pb at given $^{206}Pb/^{204}Pb$ than the NHRL (Fig. 7). There is no correlation between SiO_2 and $^{207}Pb/^{204}Pb$. The absence of crustal xenoliths excludes substantial crustal contamination of the mantle-derived magmas during fractionation of the more acidic rocks *en route* (cf. Blusztajn and Hart, 1989; Ulrych et al., 2016).

Late Cretaceous ultramafic lamprophyres, including polzenite, alnöite and related melilitolite cluster at the radiogenic end of the Pb array (Fig. 7), suggesting that their parent magma resulted from decompression melting of metasomatically enriched lithospheric mantle beneath the Bohemian Massif (cf. Embey-Isztin et al., 1993a; Riley et al., 2003; Kroner et al., 2010; Rudnick and Gao, 2014; Krmíček et al., 2016). Tertiary alkaline lamprophyres, comprising camptonite, monchiquite and related leucocratic microsyenite, which is a more felsic equivalent of alkaline lamprophyre, fall near the low-$^{206}Pb/^{204}Pb$ end-member of the mixing trend (Fig. 7). This suggests that they were produced via subsequent interaction of the lithospheric mantle with asthenosphere-derived material during the extensional phase of the Eger Rift opening (cf. Gallagher and Hawkesworth, 1992; Wilson, 1993; Harangi and Lenkey, 2007; Aghazadeh et al., 2015; Dostal et al., 2019a). Other Tertiary volcanic samples of the Bohemian Massif are distributed between above two end-members. The variations in $^{206}Pb/^{204}Pb$ do not depend on petrographic rock type or on the degree of fractionation, but instead, reflect various contributions from contrasting mantle sources during melting.

Cretaceous (pre-rift) intrusive and Quaternary (late-rift) effusive melilitites have Pb isotope compositions very similar to those of alkaline lamprophyres (Fig. 7). The Pb isotope data demonstrate that the Cretaceous melilitites (e.g., the Great Devil's Wall) did not originate from the same mantle source as the polzenites, despite emplacement in a similar tectonic stress field (Ulrych et al., 2014). The source of the melilitites was more primitive, which may have been a direct consequence of higher degree of melting (compared to the LREE enriched ultramafic lamprophyres), different melting depths, or a combination of both (cf. Hofmann, 1988; Sun and McDonough, 1989; Melluso et al., 2011).

5.3. *Regionally contrasting Pb isotope signatures in mantle-derived rocks in the Bohemian Massif*

On the scale of the Bohemian Massif, most mantle-derived rocks follow the same orogenic Pb growth curve in the $^{207}Pb/^{204}Pb$ *vs.* $^{206}Pb/^{204}Pb$ diagram (Figs. 7 and 9). As the metasomatised lithospheric mantle has higher Pb contents than the asthenospheric mantle, small or moderate contributions from other reservoirs than the lithospheric mantle may not significantly affect the Pb isotope composition of the various melts and the character of the lithospheric mantle did not change over time. The oldest mantle-derived dyke rocks emplaced during the extensional phase after the final collision of Laurussia, Gondwana and Gondwana-derived terranes are orogenic lamprophyres and lamproites (e.g., Krmíček, 2010; Krmíček et al., 2011). The orogenic Pb isotope signature as sampled by mantle-derived rocks of the Bohemian Massif since ca. 340 Myr predominantly originates from a metasomatised lithospheric mantle source affected by subduction of oceanic and continental crust during the Variscan orogeny (Krmíček et al., 2016; Dostal et al., 2019a). The lower Pb isotope ratios of Variscan lamproites and lamprophyres from the Bohemian Massif (Abdelfadil et al., 2013; Krmíček et al., 2016) do not reflect a different source than the Cretaceous to

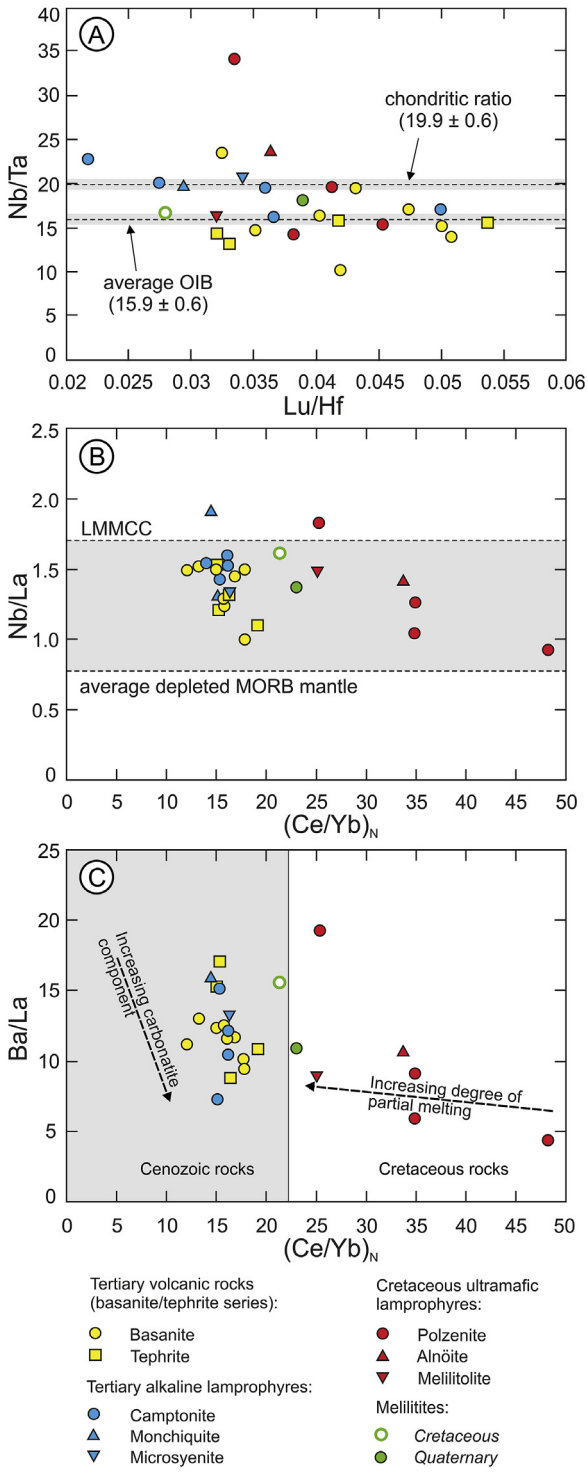

Fig. 8. Nb/Ta *vs.* Lu/Hf (A), Nb/La *vs.* $(Ce/Yb)_N$ (B) and Ba/La *vs.* $(Ce/Yb)_N$ (C) diagrams for Late Cretaceous to Cenozoic undifferentiated magmatic rocks of the Bohemian Massif. Elevated and/or variable Nb/Ta, Nb/La and $(Ce/Yb)_N$ along relatively narrow variation in Lu/Hf and Ba/La in Late Cretaceous ultramafic lamprophyres reflect low-degree partial melting of heterogeneous lithospheric mantle source (mantle component A in section 5.4). Tertiary alkaline lamprophyres and basanite/tephrite volcanic rocks show relatively constant Nb/Ta and variable Ba/La, which may indicate that their source interacted with asthenosphere-derived melts (mantle component B in section 5.4). Average OIB and chondritic Nb/Ta ratios are plotted according to Pfänder et al. (2012). Nb/La of average depleted MORB mantle and lithospheric mantle metasomatised by subducted continental crust (LMMCC) according to Workman and Hart (2005) and Borghini et al. (2018), respectively.

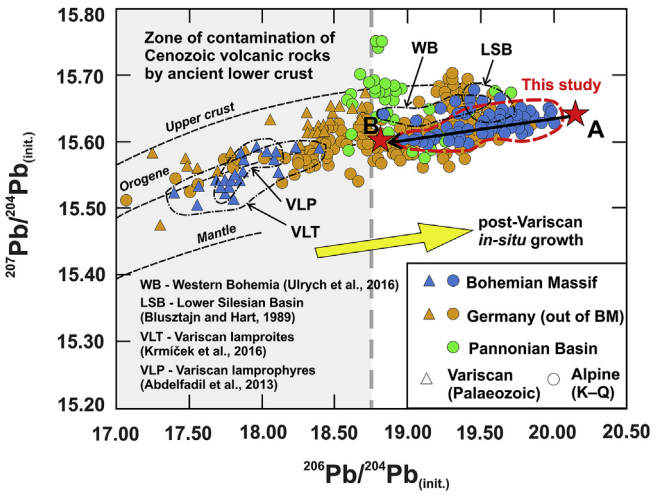

Fig. 9. Initial Pb isotope composition of Variscan and Alpine (Cretaceous to Quaternary) mantle-derived rocks from Central Europe: Bohemian Massif (Blusztajn and Hart, 1989; Haase and Renno, 2008; Abdelfadil et al., 2013; Krmíček et al., 2016; Ulrych et al., 2016), Germany, i.e., Vogelsberg (Wedepohl and Baumann, 1999; Bogaard and Wörner, 2003; Jung et al., 2011), Siebengebirge (Wedepohl and Baumann, 1999; Jung et al., 2005, 2012; Kolb et al., 2012; Schneider et al., 2016), Schwäbische Alb (Hegner et al., 1995; Wilson et al., 2004), Westerwald (Haase et al., 2004), Siebengebirge–Westerwald transition zone (Schubert et al., 2015), Kaiserstuhl (Schleicher et al., 1991), Rhön (Meyer et al., 2002; Jung et al., 2005, 2013; Mayer et al., 2013, 2014), Hegau (Wedepohl and Baumann, 1999), Heldburg (Pfänder et al., 2018), Hocheifel (Fekiacova et al., 2007), Schwarzwald (Hegner et al., 1998), Halle (Romer et al., 2001), Saar-Nahe Basin (Schmidberger and Hegner, 1999), Hessian Depression (Wedepohl and Baumann, 1999; Wedepohl, 2000), and the Carpathian-Pannonian region/Pannonian Basin (Salters et al., 1988; Embey-Isztin et al., 1993a,b; Dobosi et al., 1995; Trua et al., 2006; Harangi and Lenkey, 2007; Harangi et al., 2007). The *in situ* growth of Pb from Variscan to Mesozoic and Cenozoic mantle-derived rocks is shown schematically by a thick yellow arrow. On the contrary, the shift from more radiogenic Pb isotope compositions in the Cretaceous ultramafic lamprophyres (mantle component A) to less radiogenic Cenozoic mantle-derived rocks (mantle component B) is marked by a thin black arrow. Upper crust, orogenic and mantle growth curves are taken from Zartman and Doe (1981). Some Cenozoic rocks of the Central European Volcanic Province show conspicuously low $^{206}Pb/^{204}Pb$ ratios (<18.75) that broadly overlap with the field for Variscan samples. This relatively unradiogenic signature, accompanied by slightly enhanced $^{208}Pb/^{204}Pb$, may reflect the melting of ancient lower crustal material during magma stagnation within continental crust (e.g.,; Hegner et al., 1995; Wedepohl and Baumann, 1999; Wedepohl, 2000; Borisova et al., 2001; Bogaard and Wörner, 2003; Jung et al., 2011) or incongruent melting of Variscan metasomatised mantle rocks with clinopyroxene hosting U and Th and having more radiogenic Pb isotope composition than amphibole that is the major host of Pb (e.g., Wedepohl and Baumann, 1999; Mayer et al., 2014).

Quaternary mantle-derived rocks, but the older age of the Variscan rocks (Fig. 9).

Generally, the Pb isotope signature of off-rift volcanic rocks shows smaller contributions from the asthenospheric mantle than rocks from the rift centre (cf. Haase and Renno, 2008). For instance, tephrite from Říp Hill (sample KK2) taken at the eastern margin of the Eger Rift, ca. 30 km away from the rift centre, has the most radiogenic Pb isotope composition. Similarly, Tertiary basalts of Lower Silesia that are in an off-rift position in the possible continuation of the Eger Rift (Fig. 1A) have radiogenic Pb isotope compositions, overlapping the field occupied by ultramafic lamprophyres from the Bohemian Massif (Blusztajn and Hart, 1989). The shift towards higher $^{207}Pb/^{204}Pb$ observed for some Lower Silesia basalts (Fig. 7), however, is due to xenoliths of older crustal rocks derived from the Proterozoic basement of the East European Craton (Blusztajn and Hart, 1989).

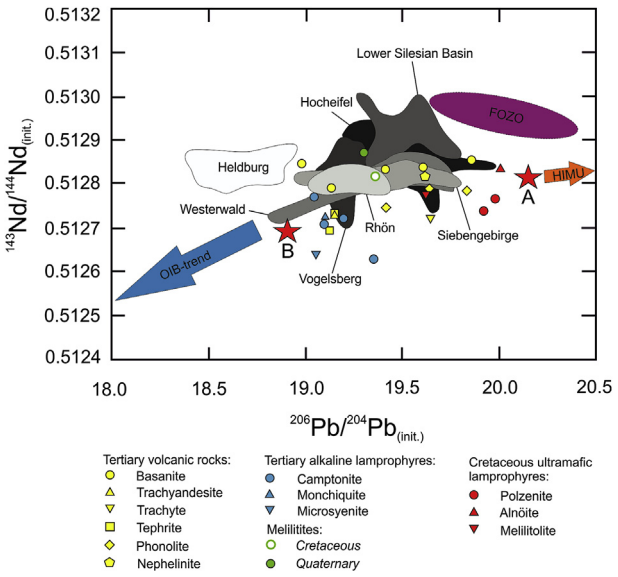

Fig. 10. Initial $^{143}Nd/^{144}Nd$ *vs.* $^{206}Pb/^{204}Pb$ diagram of investigated samples compared to major volcanic provinces of Central European Volcanic Province (CEVP). Studied samples overlap with most of the CEVP mantle-derived rocks except for the Heldburg dykes that have less radiogenic $^{206}Pb/^{204}Pb$ (see Pfänder et al., 2018 for interpretation) and mafic rocks from the Lower Silesian Basin with more radiogenic $^{143}Nd/^{144}Nd$ (Blusztajn and Hart, 1989). Late Cretaceous ultramafic lamprophyres show more radiogenic Nd–Pb signature (end-member A) trending towards high radiogenic HIMU-like mantle component, whereas Tertiary alkaline lamprophyres have less radiogenic signature (end-member B) trending towards OIB-like (non-HIMU type) mantle component. Note, the mixing trend between A and B is defined by contributions from two types of Pb-enriched lithospheric mantle. Deviations from this trend toward higher $^{143}Nd/^{144}Nd$ ratios may reflect the presence of material from the depleted mantle that has low Pb contents (and therefore does not affect the Pb isotope composition of these rocks) and sufficiently high Nd contents to shift the Nd isotope composition to more radiogenic $^{143}Nd/^{144}Nd$ ratios. Published $^{143}Nd/^{144}Nd$ ratios for samples from the same localities as samples studied in this paper are adopted from Ulrych et al. (2008), Skala et al. (2014) and Dostal et al. (2017). Compositional fields for other lavas from the CEVP are taken from Pfänder et al. (2018). Mantle components and trends (OIB, HIMU, FOZO) correspond to Stracke et al. (2005).

5.4. Lead isotope evolution of the Central European upper mantle

The lithospheric mantle beneath Variscan Europe, by and large, did not change its geochemical signature. Instead its Pb isotope signature evolved by *in situ* growth, which depends on U/Pb and Th/Pb and time. During the Alpine orogeny, however, some segments of Variscan Europe were intensely reworked, and the mantle beneath these segments may have been modified (i) by subducted crustal material during the Alpine orogeny or (ii) by significant input of asthenospheric mantle in extensional zones.

In the $^{207}Pb/^{204}Pb$ *vs.* $^{206}Pb/^{204}Pb$ diagram, mantle-derived rocks of Central Europe define a broad field that in part include rocks that have higher or lower $^{207}Pb/^{204}$ Pb at comparable $^{206}Pb/^{204}Pb$ than mantle-derived rocks from the Bohemian Massif (Fig. 9). Based on their Pb isotope compositions, two major mantle components can be distinguished. The Pb isotope signature of Late Cretaceous pre-rift ultramafic lamprophyres has the most radiogenic $^{206}Pb/^{204}Pb$ values, reflecting the lithospheric mantle metasomatised by Variscan subduction (mantle component A, Fig. 9). This is supported by the chemical composition of the rocks with strong LREE over HREE enrichment [(high $(Ce/Yb)_N$] in combination with high K_2O, Nb/Ta, and low TiO_2 and Ba/La and distinct troughs for K and Pb in primitive mantle normalised trace element plots (Figs. 5, 6A and 8). The high-radiogenic mantle component A is also prominent in the source of some off-rift volcanic areas (e.g., Blusztajn and Hart, 1989; Haase and Renno, 2008). Alpine extension within the Variscan massifs of Central Europe in the Tertiary eventually resulted in the Cenozoic rift system with widespread and voluminous volcanism in the Rhine, Ruhr Valley, and Leine grabens in Germany, and in the Eger Rift in the Bohemian Massif (Ziegler, 1992). During these events, Variscan metasomatised lithospheric mantle (component A) below the rifts was refertilised by upwelling material from the asthenosphere (Dostal et al., 2019a), which is reflected by rocks with less radiogenic $^{206}Pb/^{204}Pb$ values (Fig. 9). This mixed mantle (mantle component B) is the major source for the majority of rift-related Tertiary and Quaternary volcanic rocks of Central Europe, e.g., Vogelsberg, Siebengebirge, Schwäbische Alb, Westerwald, Kaiserstuhl, Rhön, Hegau, Heldburg as well as for volcanic rocks from the Eger Rift.

Mantle-derived rocks from the Carpathian-Pannonian region have $^{207}Pb/^{204}Pb$ values that resemble those of Siebengebirge, Kaiserstuhl, Westerwald, Siebengebirge–Westerwald transition zone and Rhön, and are slightly higher than those of corresponding rocks from the Bohemian Massif (Fig. 9). Additionally, several samples from the Carpathian-Pannonian area are characterised by $^{207}Pb/^{204}Pb$ values as high as 15.75 (Trua et al., 2006; Harangi and Lenkey, 2007). These high values reflect variable contributions from old crust.

Most volcanic rocks of CEVP fall on a two-component mixing trend in $^{143}Nd/^{144}Nd$ *vs.* $^{206}Pb/^{204}Pb$ diagram (Fig. 10). Although the Nd isotope values more or less positively correlate with the Pb isotope signature, the subtle differences in composition of the upper mantle sampled by Mesozoic and Cenozoic rocks are not so clearly documented by Nd isotopes as by Pb isotopes. Dostal et al. (2019a) demonstrated the evolution of Nd isotope composition of the upper mantle beneath Central and Western Europe from very unradiogenic values induced by the Variscan orogeny to more radiogenic values that developed during the Mesozoic rifting of the Atlantic Basin. The Nd isotope composition of Central European upper mantle was not further significantly affected since ca. 100 Ma, which is supported by studied samples. The Mesozoic to Cenozoic mantle-derived rocks are distinctly radiogenic (Ulrych et al., 2008; Skála et al., 2014; Dostal et al., 2017) compared to those of the Variscan age (Krmíček et al., 2016).

Studied mantle-derived rocks are neither overlapping, nor trending to the FOZO mantle component (Fig. 10) that isotopically overlaps with a low-velocity component (cf. Hoernle et al., 1995). This excludes an involvement of the mantle plume in their magma evolution, which is in line with seismic data from the mantle beneath the Bohemian Massif (Plomerová et al., 2007; Hrubcová et al., 2017).

6. Conclusions

Based on our Pb isotope study of mantle-derived rocks from the Bohemian Massif and their comparison with other volcanic provinces in Central Europe, we make the following conclusions:

(1) Upper Palaeozoic mantle-derived rocks demonstrate that the lithospheric mantle beneath the Bohemian Massif was metasomatised during the Variscan orogeny and received its Pb isotopic signature from subducted crustal material. Cretaceous, Tertiary and Quaternary mantle-derived rocks of the Bohemian Massif have been extracted from this mantle and, therefore, share the same crustal signature.

(2) The Pb isotope data define a two-component mixing trend. The Cretaceous ultramafic lamprophyres represent a high radiogenic end-member characterised by $^{206}Pb/^{204}Pb$ ratios up to 20.0 (Variscan metasomatised lithospheric mantle), whereas the Tertiary alkaline lamprophyres and Cretaceous and Quaternary melilitites originated from the mantle with $^{206}Pb/^{204}Pb$ ratios below 19.4 (lithospheric mantle substantially modified via interaction with the convective mantle). The Pb isotope composition of the Tertiary volcanic samples falls between these two components.

(3) Generally, off-rift volcanic/subvolcanic rocks are derived from a mantle source with higher $^{206}Pb/^{204}Pb$ than corresponding rocks from axial parts of the rift, possibly indicating that the low $^{206}Pb/^{204}Pb$ component is derived from the mantle source influenced by asthenosphere upwelling.
(4) The majority of Cenozoic mantle-derived rocks of Central Europe show similar Pb isotope variations as those of the Bohemian Massif.

Acknowledgments

This research was financially supported by the institutional project RVO 67985831 of the Institute of Geology of the Czech Academy of Sciences, as well as by the Brno University of Technology project LO1408 "AdMaS UP – Advanced Materials, Structures and Technologies", supported by the Ministry of Education, Youth and Sports of the Czech Republic under the "National Sustainability Programme I". S.K., L.K. and J.U. thank Jaroslav Dostal (Saint Mary's University, Canada) and Martin J. Timmerman (University of Potsdam, Germany) for discussion. The authors greatly appreciate an anonymous reviewer and Dr. C. Spencer for their very constructive and helpful comments and suggestions.

Appendix A. Supplementary data

Supplementary data to this article can be found online at https://doi.org/10.1016/j.gsf.2019.09.009.

References

Abdelfadil, K.M., Romer, R.L., Seifert, T., Lobst, R., 2013. Calc-alkaline lamprophyres from Lusatia (Germany) – evidence for a repeatedly enriched mantle source. Chem. Geol. 353, 230–245.
Ackerman, L., Jelínek, E., Medaris, G., Ježek, J., Siebel, W., Strnad, L., 2009. Geochemistry of Fe-rich peridotites and associated pyroxenites from Horní Bory, Bohemian Massif: insights into subduction-related melt–rock reactions. Chem. Geol. 259, 152–167.
Ackerman, L., Špaček, P., Magna, T., Ulrych, J., Svojtka, M., Hegner, E., Balogh, K., 2013. Alkaline and carbonate-rich melt metasomatism and melting of subcontinental lithospheric mantle: evidence from mantle xenoliths, NE Bavaria, Bohemian Massif. J. Petrol. 54, 2597–2633.
Ackerman, L., Ulrych, J., Řanda, Z., Erban, V., Hegner, E., Magna, T., Balogh, K., Frána, J., Lang, M., Novák, J.K., 2015. Geochemical characteristics and petrogenesis of phonolites and trachytic rocks from the České Středohoří volcanic complex, the Ohře rift, Bohemian Massif. Lithos 224–225, 256–274.
Aghazadeh, M., Prelević, D., Badrzadeh, Z., Braschi, E., van den Bogaard, P., Conticelli, S., 2015. Geochemistry, Sr–Nd–Pb isotopes and geochronology of amphibole-and mica-bearing lamprophyres in northwestern Iran: implications for mantle wedge heterogeneity in a palaeo-subduction zone. Lithos 216, 352–369.
Alibert, C., Michard, A., Albarède, F., 1983. The transitions from alkali basalts to kimberlites: isotope and trace element evidence from melilitites. Contrib. Mineral. Petrol. 82, 176–186.
Alibert, C., Leterrier, J., Panasiuk, M., Zimmermann, J.L., 1987. Trace and isotope geochemistry of the alkaline Tertiary volcanics in southwestern Poland. Lithos 20, 311–321.
Awdankiewicz, M., 2007. Late Palaeozoic lamprophyres and associated mafic subvolcanic rocks of the Sudetes (SW Poland): petrology, geochemistry and petrogenesis. Geol. Sudet. 39, 11–99.
Awdankiewicz, M., Awdankiewicz, H., Kryza, R., Rodionov, N., Timmerman, M.J., 2009. Ar-Ar and SHRIMP constraints on the age of Late Palaeozoic intermediate and silicic dykes and sills in the Sudetes. Mineralogia, Special Papers 34, 9.
Babuška, V., Plomerová, J., 1992. The lithosphere in central Europe – seismological and petrological aspects. Tectonophysics 207, 141–163.
Babuška, V., Plomerová, J., 2001. Subcrustal lithosphere around the Saxothuringian–Moldanubian Suture Zone – a model derived from anisotropy of seismic wave velocities. Tectonophysics 332, 185–199.
Babuška, V., Plomerová, J., 2010. Mantle lithosphere control of crustal tectonics and magmatism of the westerm Ohře (Eger) Rift. J. Geosci. 55, 171–186.
Bendl, J., Vokurka, K., Sundvoll, B., 1993. Strontium and neodymium isotope study of Bohemian basalts. Mineral. Petrol. 48, 35–45.
Benek, R., Kramer, W., McCann, T., Scheck, M., Negendank, J.F.W., Korich, D., Huebscher, H.-D., Bayer, U., 1996. Permo-Carboniferous magmatism of the northeast German basin. Tectonophysics 266, 379–404.
Berkesi, M., Czuppon, G., Szabó, C., Kovács, I., Ferrero, S., Boiron, M.C., Peiffert, C., 2019. Pargasite in fluid inclusions of mantle xenoliths from northeast Australia (Mt. Quincan): evidence of interaction with asthenospheric fluid. Chem. Geol. 508, 182–196.
Blusztajn, J., Hart, S.R., 1989. Sr, Nd and Pb isotopic character of Tertiary basalts from southwest Poland. Geochem. Cosmochim. Acta 53, 2689–2696.
Blusztajn, J., Hegner, E., 2002. Osmium isotopic systematics of melilitites from the Tertiary central European volcanic province in SW Germany. Chem. Geol. 189, 91–103.
Bogaard, P.J.F., Wörner, G., 2003. Petrogenesis of basanitic to tholeiitic volcanic rocks from the Miocene Vogelsberg, Central Germany. J. Petrol. 44, 569–602.
Borghini, A., Ferrero, S., Wunder, B., Laurent, O., O'Brien, P.J., Ziemann, M.A., 2018. Granitoid melt inclusions in orogenic peridotite and the origin of garnet clinopyroxenite. Geology 46, 1007–1010.
Borisova, A.Yu, Belyatsky, B.V., Portnyagin, M.V., Sushchevskaya, N.M., 2001. Petrogenesis of olivine-phyric basalts from the Aphanasey Nikitin Rise: evidence for contamination by cratonic lower continental crust. J. Petrol. 42, 277–319.
Boynton, W.V., 1984. Cosmochemistry of the rare earth elements: meteorite studies. Dev. Geochem. 2, 63–114.
Cajz, V., Rapprich, V., Erban, V., Pécskay, Z., Radoň, M., 2009. Late Miocene volcanic activity in the České středohoří mountains (Ohře/Eger graben, northern Bohemia). Geol. Carpathica 60, 519–533.
Cebrià, J.M., Wilson, M., 1995. Cenozoic mafic magmatism in Western/Central Europe: a common European asthenospheric reservoir. Terra Nova Abstract Suplement, 7, 162.
Class, C., Goldstein, S.L., 1997. Plume-lithosphere interactions in the ocean basins: constraints from the source mineralogy. Earth Planet. Sci. Lett. 150, 245–260.
Cohen, R.S., O'Nions, R.K., 1982. Identification of recycled continental material in the mantle from Sr, Nd and Pb isotope investigations. Earth Planet. Sci. Lett. 61, 73–84.
Conticelli, S., D'Antonio, M., Pinarelli, L., Civetta, L., 2002. Source contamination and mantle heterogeneity in the genesis of Italian potassic and ultrapotassic volcanic rocks: Sr–Nd–Pb isotope data from Roman Province and Southern Tuscany. Mineral. Petrol. 74, 189–222.
Davies, G.R., Macdonald, R., 1987. Crustal influences in the petrogenesis of the Naivasha Basalt–Comendite Complex: combined trace element and Sr–Nd–Pb isotope constraints. J. Petrol. 28, 1009–1031.
Dèzes, P., Schmid, S.M., Ziegler, P.A., 2004. Evolution of the European Cenozoic rift system: interaction of the Alpine and Pyrenean orogens with their foreland lithosphere. Tectonophysics 389, 1–33.
Dobosi, G., Fodor, R.V., Goldberg, S.A., 1995. Late-Cenozoic alkali basalt magmatism in Northern Hungary and Slovakia: petrology, source compositions and relationship to tectonics. Acta Vulcanol. 7, 199–207.
Dostal, J., Murphy, J.B., Shellnutt, J.G., 2019a. Secular isotopic variation in lithospheric mantle through the Variscan orogen: Neoproterozoic to Cenozoic magmatism in continental Europe. Geology 47, 637–640.
Dostal, J., Murphy, J.B., Shellnutt, J.G., Ulrych, J., Fediuk, F., 2019b. Neoproterozoic to Cenozoic magmatism in the central part of the Bohemian Massif (Czech Republic): isotopic tracking of the evolution of the mantle through the Variscan orogeny. Lithos 326, 358–369.
Dostal, J., Shellnutt, J.G., Ulrych, J., 2017. Petrogenesis of the Cenozoic alkaline volcanic rock series of the České Středohoří Complex (Bohemian Massif), Czech Republic: a case for two lineages. Am. J. Sci. 317, 677–706.
Downes, H., 2001. Formation and modification of the shallow sub-continental lithospheric mantle: a review of geochemical evidence from ultramafic xenolith suites and tectonically emplaced ultramafic massifs of western and central Europe. J. Petrol. 42, 233–250.
Embey-Isztin, A., Dobosi, G., James, D., Downes, H., Poultidis, C., Scharbert, H.G., 1993a. A compilation of new major, trace element and isotope geochemical analyses of the young alkali basalts from the Pannonian Basin. Fragmenta Geologica et Petrographica 16, 5–26.
Embey-Isztin, A., Downes, H., James, D.E., Upton, B.G.J., Dobosi, G., Ingram, G.A., Harmon, R.S., Scharbert, H.G., 1993b. The petrogenesis of Pliocene alkaline volcanic rocks from the Pannonian Basin, eastern central Europe. J. Petrol. 34, 317–343.
Fekiacova, Z., Mertz, D.F., Hofmann, A.W., 2007. Geodynamic setting of the Tertiary Hocheifel volcanism (Germany), part II: geochemistry and Sr, Nd and Pb isotopic compositions. In: Ritter, J.R.R., Christensen, U.R. (Eds.), Mantle Plumes – A Multidisciplinary Approach. Springer, Berlin, pp. 207–239.
Ferrero, S., O'Brien, P.J., Borghini, A., Wunder, B., Wälle, M., Günter, C., Ziemann, M.A., 2018. A treasure chest full of nanogranitoids: an archive to investigate crustal melting in the Bohemian Massif. Geological Society, London, Special Publications 478, 13–38.
Gallagher, K., Hawkesworth, C., 1992. Dehydration melting and the generation of continental flood basalts. Nature 358, 57–59.
Haase, K.M., Beier, C., Regelous, M., Rapprich, V., Renno, A., 2017. Spatial variability of source composition and petrogenesis in rift and rift flank alkaline lavas from the Eger Rift, Central Europe. Chem. Geol. 455, 304–314.
Haase, K.M., Goldschmidt, B., Garbe-Schönberg, C.D., 2004. Petrogenesis of Tertiary continental intra-plate lavas from the Westerwald region, Germany. J. Petrol. 45, 883–905.
Haase, K.M., Renno, A.D., 2008. Variation of magma generation and mantle sources during continental rifting observed in Cenozoic lavas from the Eger Rift, Central Europe. Chem. Geol. 257, 195–205.
Harangi, S., Downes, H., Thirlwall, M., Gméling, K., 2007. Geochemistry, petrogenesis and geodynamic relationships of Miocene calc-alkaline volcanic rocks in the Western Carpathian arc, eastern central Europe. J. Petrol. 48, 2261–2287.
Harangi, S., Lenkey, L., 2007. Genesis of the Neogene to Quaternary volcanism in the Carpathian-Pannonian region: role of subduction, extension, and mantle plume. Geol. Soc. Am. Spec. Pap. 418, 67–92.
Hart, S.R., 1984. A large-scale isotope anomaly in the Southern Hemisphere mantle. Nature 309, 753–757.

Hegner, E., Kölbl-Ebert, M., Loeschke, J., 1998. Post-collisional Variscan lamprophyres (Black Forest, Germany): $^{40}Ar/^{39}Ar$ phlogopite dating, Nd, Pb, Sr isotope, and trace element characteristics. Lithos 45, 395–411.
Hegner, E., Walter, H.J., Satir, M., 1995. Pb–Sr–Nd isotopic compositions and trace element geochemistry of megacrysts and melilitites from the Tertiary Urach volcanic field: source composition of small volume melts under SW Germany. Contrib. Mineral. Petrol. 122, 322–335.
Hoernle, K., Zhang, Y.-S., Graham, D., 1995. Seismic and geochemical evidence for large-scale mantle upwelling beneath the eastern Atlantic and western and central Europe. Nature 374, 34–39.
Hofmann, A.W., 1988. Chemical differentiation of the Earth: the relationship between mantle, continental crust, and oceanic crust. Earth Planet. Sci. Lett. 90, 297–314.
Hrouda, F., Verner, K., Kubínová, Š., Buriánek, D., Faryad, S.W., Chlupáčová, M., Holub, F.V., 2016. Magnetic fabric and emplacement of dykes of lamprophyres and related rocks of the central Bohemian dyke swarm (central European variscides). J. Geosci. 61, 335–354.
Hrubcová, P., Geissler, W.H., Bräuer, K., Vavryčuk, V., Tomek, Č., Kämpf, H., 2017. Active magmatic underplating in western Eger Rift, central Europe. Tectonics 36, 2846–2862.
Jung, S., Mezger, K., Hauff, F., Pack, A., Hoernes, S., 2013. Petrogenesis of rift-related tephrites, phonolites and trachytes (central European volcanic province, Rhön, FRG): constraints from Sr, Nd, Pb and O isotopes. Chem. Geol. 354, 203–215.
Jung, S., Pfänder, J.A., Brauns, M., Maas, R., 2011. Crustal contamination and mantle source characteristics in continental intra-plate volcanic rocks: Pb, Hf and Os isotopes from central European volcanic province basalts. Geochem. Cosmochim. Acta 75, 2664–2683.
Jung, S., Pfänder, J.A., Brügmann, G., Stracke, A., 2005. Sources of primitive alkaline volcanic rocks from the Central European Volcanic Province (Rhön, Germany) inferred from Hf, Os and Pb isotopes. Contrib. Mineral. Petrol. 150, 546–559.
Jung, S., Vieten, K., Romer, R.L., Mezger, K., Hoernes, S., Satir, M., 2012. Petrogenesis of Tertiary alkaline magmas in the Siebengebirge, Germany. J. Petrol. 53, 2381–2409.
Kalvoda, J., Bábek, O., 2010. The margins of Laurussia in central and southeast Europe and southwest Asia. Gondwana Res. 17, 526–545.
Kalvoda, J., Bábek, O., Fatka, O., Leichmann, J., Melichar, R., Nehyba, S., Špaček, P., 2008. Brunovistulian terrane (Bohemian massif, central Europe) from late Proterozoic to late Paleozoic: a review. Int. J. Earth Sci. 97, 497–518.
Kolb, M., Paulick, H., Kirchenbaur, M., Münker, C., 2012. Petrogenesis of mafic to felsic lavas from the Oligocene Siebengebirge volcanic field (Germany): implications for the origin of intracontinental volcanism in Central Europe. J. Petrol. 53, 2349–2379.
Krmíček, L., 2010. Pre-Mesozoic lamprophyres and lamproites of the Bohemian massif (Czech Republic, Poland, Germany, Austria). Mineralogia, Special Papers 37, 37–46.
Krmíček, L., Cempírek, J., Havlín, A., Přichystal, A., Houzar, S., Krmíčková, M., Gadas, P., 2011. Mineralogy and petrogenesis of a Ba–Ti–Zr-rich peralkaline dyke from Šebkovice (Czech Republic): recognition of the most lamproitic Variscan intrusion. Lithos 121, 74–86.
Krmíček, L., Halavínová, M., Romer, R.L., Galiová, M.V., Vaculovič, T., 2014. Phlogopite/matrix, clinopyroxene/matrix and clinopyroxene/phlogopite trace-element partitioning in a calc-alkaline lamprophyre: new constrains from the Křižanovice minette dyke (Bohemian Massif). J. Geosci. 59, 87–96.
Krmíček, L., Romer, R.L., Ulrych, J., Glodny, J., Prelević, D., 2016. Petrogenesis of orogenic lamproites of the Bohemian Massif: Sr–Nd–Pb–Li isotope constraints for Variscan enrichment of ultra-depleted mantle domains. Gondwana Res. 35, 198–216.
Kroner, U., Hahn, T., Romer, R.L., Linnemann, U., 2007. The Variscan orogeny in the Saxo-Thuringian zone – heterogenous overprint of Cadomian/Paleozoic Peri-Gondwana crust. Geol. Soc. Am. Spec. Pap. 423, 153–172.
Kroner, U., Linnemann, U., Romer, R.L., 2010. The Saxo-Thuringian zone of the Variscan orogen as part of Pangea. In: Linnemann, U., Romer, R.L. (Eds.), Pre-Mesozoic Geology of Saxo-Thuringia – from the Cadomian Active Margin to the Variscan Orogen. Schweizerbart, Stuttgart, pp. 171–192.
Kroner, U., Romer, R.L., 2010. The Saxo-Thuringian Zone – tip of the Armorican spur and part of the Gondwana plate. In: Linnemann, U., Romer, R.L. (Eds.), Pre-Mesozoic Geology of Saxo-Thuringia: from the Cadomian Active Margin to the Variscan Orogen. Schweizerbart, Stuttgart, pp. 371–394.
Kroner, U., Romer, R.L., 2013. Two plates – many subduction zones: the Variscan orogeny reconsidered. Gondwana Res. 24, 298–329.
Kroner, U., Roscher, M., Romer, R.L., 2016. Ancient plate kinematics derived from the deformation pattern of continental crust: paleo-and Neo-Tethys opening coeval with prolonged Gondwana–Laurussia convergence. Tectonophysics 681, 220–233.
Le Maitre, R.W., 2002. Igneous Rocks: A Classification and Glossary of Terms: Recommendations of the International Union of Geological Sciences Subcommission on the Systematics of Igneous Rocks, second ed. Cambridge University Press, Cambridge, 256 pp.
Leake, B.E., 21 authors, 1997. Nomenclature of amphiboles: report of the subcommittee on amphiboles of the international mineralogical association commission on new minerals and mineral names. Mineral. Mag. 61, 295–321.
Lorenz, V., Nicholls, I.A., 1984. Plate and intraplate processes of Hercynian Europe during the late Paleozoic. Tectonophysics 107, 25–56.
Lustrino, M., Wilson, M., 2007. The circum-Mediterranean anorogenic Cenozoic igneous province. Earth Sci. Rev. 81, 1–65.
Mayer, B., Jung, S., Romer, R.L., Pfänder, J.A., Klügel, A., Pack, A., Gröner, E., 2014. Amphibole in alkaline basalts from intraplate settings: implications for the petrogenesis of alkaline lavas from the metasomatised lithospheric mantle. Contrib. Mineral. Petrol. 167, 989.
Mayer, B., Jung, S., Romer, R.L., Stracke, A., Haase, K.M., Garbe-Schönberg, C.D., 2013. Petrogenesis of Tertiary hornblende-bearing lavas in the Rhön, Germany. J. Petrol. 54, 2095–2123.
McCann, T., Pascal, C., Timmerman, M.J., Krzywiec, P., López-Gómez, J., Wetzel, L., Krawczyk, C.M., Rieke, H., Lamarche, J., 2006. Post-Variscan (end Carboniferous-Early Permian) basin evolution in western and central Europe. Geological Society, London, Memoirs 32, 355–388.
McDonough, W.F., Sun, S.S., 1995. The composition of the Earth. Chem. Geol. 120, 223–253.
Meier, T., Soomro, R.A., Viereck, L., Lebedev, S., Behrmann, J.H., Weidle, C., Cristiano, L., Hanemann, R., 2016. Mesozoic and Cenozoic evolution of the central European lithosphere. Tectonophysics 692, 58–73.
Melluso, L., le Roex, A.P., Morra, V., 2011. Petrogenesis and Nd-, Pb-, Sr-isotope geochemistry of the Cenozoic olivine melilitites and olivine nephelinites ("*ankaratrites*") in Madagascar. Lithos 127, 505–521.
Merlet, C., 1992. Quantitative electron probe microanalysis: new accurate Φ (ρz) description. Microchimica Acta 12, 107–115.
Meyer, R., Abratis, M., Viereck-Götte, L., Mädler, J., Hertogen, J., Romer, R.L., 2002. Mantelquellen des Vulkanismus in der thüringischen Rhön. Beiträge zur Geologie von Thüringen 9, 75–105 (in German).
Morimoto, N., 1988. Nomenclature of pyroxenes. Mineral. Petrol. 39, 55–76.
Neumann, E.R., Wilson, M., Heeremans, M., Spencer, E.A., Obst, K., Timmerman, M.J., Kirstein, L., 2004. Carboniferous-Permian rifting and magmatism in southern Scandinavia, the North Sea and northern Germany: a review. Geological Society, London, Special Publications 223, 11–40.
Nowell, D.A., Jones, M.C., Pyle, D.M., 2006. Episodic Quaternary volcanism in France and Germany. J. Quat. Sci. 21, 645–675.
Pfänder, J.A., Jung, S., Münker, C., Stracke, A., Mezger, K., 2012. A possible high Nb/Ta reservoir in the continental lithospheric mantle and consequences on the global Nb budget –Evidence from continental basalts from Central Germany. Geochem. Cosmochim. Acta 77, 232–251.
Pfänder, J.A., Jung, S., Klügel, A., Münker, C., Romer, R.L., Sperner, B., Rohrmüller, J., 2018. Recurrent local melting of metasomatised lithospheric mantle in response to continental rifting: constraints from basanites and nephelinites/melilitites from SE Germany. J. Petrol. 59, 667–694.
Pin, C., Waldhausrová, J., 2007. Sm-Nd isotope and trace element study of Late Proterozoic metabasalts ("spilites") from the Central Barrandian domain (Bohemian Massif, Czech Republic). Geol. Soc. Am. Spec. Pap. 423, 231–247.
Plomerová, J., Achauer, U., Babuška, V., Vecsey, L., BOHEMA working group, 2007. Upper mantle beneath the Eger Rift (central Europe): plume or asthenosphere upwelling? Geophys. J. Int. 169, 675–682.
Prodehl, C., Mueller, S., Haak, V., 2006. The European Cenozoic rift system. Dev. Geotectonics 25, 133–212.
Rapprich, V., 2005. Compositional variation of clinopyroxenes of basaltic, essexitic and tephriphonolitic rocks from the Doupovské hory Volcanic Complex, NW Bohemia. J. Geosci. 50, 119–132.
Rieder, M., 14 authors, 1998. Nomenclature of the micas. Clays and Clay Miner. 46, 586–595.
Riley, T.R., Leat, P.T., Storey, B.C., Parkinson, I.J., Millar, I.L., 2003. Ultramafic lamprophyres of the Ferrar large igneous province: evidence for a HIMU mantle component. Lithos 66, 63–76.
Rock, N.M.S., 1991. Lamprophyres. Springer, New York, 285 pp.
Romer, R.L., Förster, H.J., Breitkreuz, C., 2001. Intracontinental extensional magmatism with a subduction fingerprint: the late Carboniferous Halle Volcanic Complex (Germany). Contrib. Mineral. Petrol. 141, 201–221.
Romer, R.L., Heinrich, W., Schröder-Smeibidl, B., Meixner, A., Fischer, C.O., Schulz, C., 2005. Elemental dispersion and stable isotope fractionation during reactive fluid-flow and fluid immiscibility in the Bufa del Diente aureole, NE-Mexico: evidence from radiographies and Li, B, Sr, Nd, and Pb isotope systematics. Contrib. Mineral. Petrol. 149, 400–429.
Rudnick, R.L., Gao, S., 2014. Composition of the continental crust. In: Holland, H., Turekian, K. (Eds.), Treatise on Geochemistry, vol. 4. Elsevier, Amsterdam, pp. 1–51.
Salters, V.J.M., Hart, S.R., Pantó, G., 1988. Origin of Late Cenozoic Volcanic Rocks of the Carpathian Arc, Hungary, vol 45. American Association of Petroleum Geologists, Memoir, pp. 279–292.
Schleicher, H., Baumann, A., Keller, J., 1991. Pb isotopic systematics of alkaline volcanic rocks and carbonatites from the Kaiserstuhl, upper Rhine rift valley. F.R.G. Chemical geology 93, 231–243.
Schmidberger, S.S., Hegner, E., 1999. Geochemistry and isotope systematics of calc-alkaline volcanic rocks from the Saar-Nahe basin (SW Germany) – implications for Late-Variscan orogenic development. Contrib. Mineral. Petrol. 135, 373–385.
Schneider, K.P., Kirchenbaur, M., Fonseca, R.O.C., Kasper, H.U., Münker, C., Froitzheim, N., 2016. Role of crustal assimilation and basement compositions in the petrogenesis of differentiated intraplate volcanic rocks: a case study from the Siebengebirge Volcanic Field, Germany. Contrib. Mineral. Petrol. 171, 58.
Schubert, S., Jung, S., Pfänder, J.A., Hauff, F., Garbe-Schönberg, D., 2015. Petrogenesis of Tertiary continental intra-plate lavas between Siebengebirge and Westerwald, Germany: constraints from trace element systematics and Nd, Sr and Pb isotopes. J. Volcanol. Geotherm. Res. 305, 84–99.
Sharygin, V.V., Kamenetsky, V.S., Kamenetsky, M.B., 2008. Potassium sulfides in kimberlite-hosted chloride–"nyerereite" and chloride clasts of Udachnaya-East pipe, Yakutia, Russia. Can. Mineral. 46, 1079–1095.
Skála, R., Ulrych, J., Ackerman, L., Jelínek, E., Dostal, J., Hegner, E., Řanda, Z., 2014. Tertiary alkaline Roztoky intrusive complex: České středohoří Mts., Czech Republic: petrogenetic characteristics. Int. J. Earth Sci. 103, 1233–1262.
Skála, R., Ulrych, J., Krmíček, L., Fediuk, F., Ackerman, L., Balogh, K., 2015. Upper Cretaceous to Pleistocene melilitic volcanic rocks of the Bohemian Massif: petrology and mineral chemistry. Geol. Carpathica 66, 197–216.

Stracke, A., Hofmann, A.W., Hart, S.R., 2005. FOZO, HIMU, and the rest of the mantle zoo. Geochem. Geophys. Geosyst. 6, 5.
Sun, S.S., McDonough, W.S., 1989. Chemical and isotopic systematics of oceanic basalts: implications for mantle composition and processes. Geological Society, London, Special Publications 42, 313–345.
Špaček, P., Sýkorová, Z., Pazdírková, J., Švancara, J., Havíř, J., 2011. Present-day seismicity of the south-eastern Elbe Fault System (NE Bohemian massif). Studia Geophysica et Geodetica 50, 233–258.
Timmerman, M.J., 2008. Palaeozoic magmatism. In: McCann, T. (Ed.), The Geology of Central Europe, Volume 1. Precambrian and Palaeozoic. Geological Society of London, London, United Kingdom, pp. 665–748.
Timmerman, M.J., Heeremans, M., Kirstein, L.A., Larsen, B.T., Spencer-Dunworth, E.A., Sundvoll, B., 2009. Linking changes in tectonic style with magmatism in northern Europe during the late Carboniferous to latest Permian. Tectonophysics 473, 375–390.
Trua, T., Serri, G., Birkenmajer, K., Pécskay, Z., 2006. Geochemical and Sr–Nd–Pb isotopic compositions of Mts Pieniny dykes and sills (West Carpathians): evidence for melting in the lithospheric mantle. Lithos 90, 57–76.
Ulrych, J., Ackerman, L., Balogh, K., Hegner, E., Jelínek, E., Pécskay, Z., Přichystal, A., Upton, B.G.J., Zimák, J., Foltýnová, R., 2013. Plio-Pleistocene basanitic and melilititic series of the Bohemian Massif: K-Ar ages, major/trace element and Sr–Nd isotopic data. Chem. Erde 73, 429–450.
Ulrych, J., Adamovič, J., Krmíček, L., Ackerman, L., Balogh, K., 2014. Revision of Scheumann's classification of melilitic lamprophyres and related melilitic rocks in light of new analytical data. J. Geosci. 59, 3–22.
Ulrych, J., Dostal, J., Hegner, E., Balogh, K., Ackerman, L., 2008. Late Cretaceous to Paleogene melilitic rocks of the Ohře/Eger rift in northern Bohemia, Czech Republic: insights into the initial stages of continental rifting. Lithos 101, 141–161.
Ulrych, J., Dostal, J., Adamovič, J., Jelínek, E., Špaček, P., Hegner, E., Balogh, K., 2011. Recurrent Cenozoic volcanic activity in the Bohemian massif (Czech Republic). Lithos 123, 133–144.
Ulrych, J., Krmíček, L., Tomek, Č., Lloyd, F.E., Ladenberger, A., Ackerman, L., Balogh, K., 2016. Petrogenesis of Miocene alkaline volcanic suites from western Bohemia: whole rock geochemistry and Sr–Nd–Pb isotopic signatures. Chemie der Erde – Geochemistry 76, 77–93.
Ulrych, J., Krmíček, L., Teschner, C., Skála, R., Adamovič, J., Ďurišová, J., Křížová, Š., Kubošková, S., Radoň, M., 2018. Chemistry and Sr–Nd isotope signature of amphiboles of the magnesio-hastingsite–pargasite–kaersutite series in Cenozoic volcanic rocks: insight into lithospheric mantle beneath the Bohemian Massif. Lithos 312–313, 308–321.
Ulrych, J., Pivec, E., 1997. Age-related contrasting alkaline volcanic series in North Bohemia. Chemie der Erde – Geochemistry 57, 311–336.
Ulrych, J., Pivec, E., Jelínek, E., Arva-Sos, E., Bendl, J., 1998. Geochemically anomalous olivine-poor nephelinite of Říp hill, Czech Republic. J. Geosci. 43, 299–311.
Ulrych, J., Svobodová, J., Balogh, K., 2002. The source of Cenozoic volcanism in the České středohoří Mts., Bohemian massif. Neues Jahrb. Mineral. Abh. 177, 133–162.
Velázquez, V.F., Fonseca Giannini, P.C., Riccomini, C., Martins Sallun, A.E., Hachiro, J., de Barros Gomes, C., 2008. Columnar joints in the Patiño formation sandstones, eastern Paraguay: a dynamic interaction between dyke intrusion, quartz dissolution and cooling-induced fractures. Episodes 31, 302–308.
Vokurka, K., 1997. Neodymium and strontium isotopes of basalts from the Doupovské hory Mts., Bohemia. J. Czech Geol. Soc. 42, 17.
Wedepohl, K.H., 2000. The composition and formation of Miocene tholeiites in the Central European Cenozoic plume volcanism (CECV). Contrib. Mineral. Petrol. 140, 180–189.
Wedepohl, K.H., Baumann, A., 1999. Central European Cenozoic plume volcanism with OIB characteristics and indications of a lower mantle source. Contrib. Mineral. Petrol. 136, 225–239.
Wedepohl, K.H., Gohn, E., Hartmann, G., 1994. Cenozoic alkali basaltic magma of western Germany and their products of differentiation. Contrib. Mineral. Petrol. 115, 253–278.
White, R., McKenzie, D., 1989. Magmatism at rift zones: the generation of volcanic continental margins and flood basalts. J. Geophys. Res.: Solid Earth 94, 7685–7729.
Wilson, M., 1993. Geochemical signatures of oceanic and continental basalts: a key to mantle dynamics? J. Geol. Soc. 150, 977–990.
Wilson, M., Downes, H., 1991. Tertiary-Quaternary extension-related alkaline magmatism in western and central Europe. J. Petrol. 32, 811–849.
Wilson, M., Downes, H., 1992. Mafic alkaline magmatism associated with the European Cenozoic rift system. Tectonophysics 208, 173–182.
Wilson, M., Neumann, E.R., Davies, G.R., Timmerman, M.J., Heeremans, M., Larsen, B.T., 2004. Permo-Carboniferous magmatism and rifting in Europe: introduction. Geological Society, London, Special Publications 223, 1–10.
Wilson, M., Paterson, R., 2001. Intraplate magmatism related to short-wavelength convective instabilities in the upper mantle: evidence from the Tertiary–Quaternary volcanic province of western and central Europe. Geol. Soc. Am. Spec. Pap. 352, 37–58.
Witt-Eickschen, G., Kramm, U., 1997. Mantle upwelling and metasomatism beneath Central Europe: geochemical and isotopic constraints from mantle xenoliths from the Rhön (Germany). J. Petrol. 38, 479–493.
Workman, R.K., Hart, S.R., 2005. Major and trace element composition of the depleted MORB mantle (DMM). Earth Planet. Sci. Lett. 231, 53–72.
Zachariáš, J., Adamovič, J., Konečný, P., 2008. The uraninite–pyrite association, a sensitive indicator of changes in paleofluid composition: an example from the Ohře (Eger) Graben, Bohemian Massif, Czech Republic. Can. Mineral. 46, 1159–1172.
Zartman, R.E., Doe, B.R., 1981. Plumbotectonics – the model. Tectonophysics 75, 135–162.
Ziegler, P.A., 1992. European Cenozoic rift system. Tectonophysics 208, 91–111.
Ziegler, P.A., 1994. Cenozoic Rift system of western and central Europe – an overview. Geol. Mijnb. 73, 99–127.
Zou, H., Zindler, A., Xu, X., Qi, Q., 2000. Major, trace element, and Nd, Sr and Pb isotope studies of Cenozoic basalts in SE China: mantle sources, regional variations, and tectonic significance. Chem. Geol. 171, 33–47.
Žák, J., Sláma, J., 2018. How far did the Cadomian 'terranes' travel from Gondwana during early Palaeozoic? A critical reappraisal based on detrital zircon geochronology. Int. Geol. Rev. 60, 319–338.